Sudan University of Science and Technology

College of Graduate Studies

Determination of Some Optical and Electrical Properties for Fe Oxide Doped by Al and Cu Using X-Ray Diffraction and Ultra Violet Spectrometer

تحديد بعض الخواص الضوئية والكهربية لأوكسيد الحديد المطعم بالألمونيوم والنحاس باستخدام حيود الأشعة السينية و مطياف الأشعة فوق البنفسجية

A thesis submitted for the Fulfillment of the Award of PhD in Physics

By

Mahmoud Bashir Ali Dawra

Supervisor

Professor Mubarak Dirar Abd-Alla Yagoub

February 2023

بسم الله الرحمن الرحيم

قَالَ تَعَالَىٰ:

﴿ قَالُوا۟ سُبْحَٰنَكَ لَا عِلْمَ لَنَآ إِلَّا مَا عَلَّمْتَنَآ ۖ إِنَّكَ أَنتَ ٱلْعَلِيمُ ٱلْحَكِيمُ ﴿٣٢﴾ ﴾

صدق الله العظيم

Dedication

Dedicated to my parents, my family, my brothers and my sister

I would like to dedicate these work teachers

Acknowledgement

I would like to thank God for helping me to do this work. Thanks, extends also to Sudan University of Science and Technology, graduate college, faculty of science, and department of physics for hospitality.

I would like to express my gratitude to my supervisor **Prof. D r. Mubarak Dirar Abdulla** for useful advice and fruitful suggestions.

I would like to thank and **Dr. Abdalsakhi sulaiman** at Alneelain University of Science & Technology for helping in doing the experimental part of this research.

Abstract

The energy problem is one of the long standing problems facing civilization. This problem can be solved mainly using solar cells. Unfortunately, these cells suffer from their low efficiency. To solve this problem many solar cell thin films were fabricated. The aim of this work is to fabricate some solar thin films to study their optical and electrical properties using UV and FTIR spectrometers. Their Nano and crystal structure were studied using XRD technique. To do this five samples of $Al_{2x}\ Fe_{3(1-x)}O_4$ and five samples of $Cu_xFe_{1-x}\ O_2$ were prepared with molar concentration indexes x (0.1, 0.3, 0.5,0.7, 0.9). The preparation technique is called Sol gel method. In this technique Al, Cu and Fe oxides were dissolved separately in distilled water in acidic medium separately. Then Al solution was mixed with Fe and Cu solution was mixed with Fe also separately. The samples are then dried in oven. The results of XRD shows increase of crystal Nano size upon decreasing Al and Cu molar concentrations. The results of UV indicate decrease of energy gap for all samples upon decreasing the Nano crystal size. The increase of Nano crystal size for Al increases the refractive index, optical and electrical conductivity beside the electric permittivity. However, for Cu the increase of the Nano crystal size decreases the refractive index, optical and electrical conductivity, beside the electric permittivity, while it causes the magnetic permeability to increase the FTIR results shows existence of many bonds that can absorb light and vibrate to give charge carriers more energies. This means that $CuFe_3O_2$ samples can give more efficient solar cells, since decreasing the Cu Nano size decreases the energy gap and increasing the conductivity in contrast to $Al_{2x}Fe_{3(1-x)}O_4$ samples in which the conductivity decreases.

مستخلص

تعتبر مشكلة الطاقة من أحد المشاكل المزمنة التي تواجه المدنية الحديثة. ويمكن حل هذه المشكلة بصورة جذرية باستخدام الخلايا الشمسية. ولسوء الحظ تعاني هذه الخلايا من تدني الكفاءة. ولعلاج هذه المشكلة تم تصنيع خلايا شمسية عديدة في هيئة شرائح دقيقة. الغرض من هذا العمل هو تصنيع عدة أغشية دقيقة شمسية لدراسة خواصها الضوئية والكهربية باستخدام مطياف الأشعة فوق البنفسجية ومطياف تحويل فورير للأشعة تحت الحمراء. ولدراسة تركيبها النانوي والبلوري تم استخدام تقنية حيود الأشعة السينية. للقيام بذلك تم تحضير 5 عينات من $Al_{2x}\ Fe_{3(1-x)}O_4$ وكذلك 5 عينات من Cu_xFe_{1-x} O_2 بمعاملات تركيز x (0.1, 0.3, 0.5,0.7,0.9). تسمى تقنية التحضير بطريقة المحلول الجلاتيني . في هذه التقنية تمت إذابة كل من اوكسيد الألمونيوم و النحاس و الحديد بصورة منفصلة في محلول مائي مقطر في وسط حمضي . ثم خُلط محلول الألمونيوم مع الحديد و خُلط محلول النحاس مع الحديد بصورة منفصلة و تم تجفيف العينات في فرن . أوضحت نتائج حيود الأشعة السينية نقصان البعد النانوي البلوري بزيادة تركيزاتAl و *Cu* الجزيئية. وبينت نتائج الأشعة فوق البنفسجية نقصان فجوة الطاقة بنقصان البعد النانوي البلوري. وبينت كذلك أن زيادة البعد النانوي ل Al يزيد معامل الانكسار والموصلية الضوئية والكهربية والسماحية الكهربية. ولكن زيادة البعد النانوي البلوري لـ *Cu* يؤدي لنقصان معامل الانكسار والموصلية الضوئية والكهربية والمساحية الكهربية. وقد بينت نتائج الأشعة تحت الحمراء وجود روابط عديدة يمكن أن تمتص الضوء وتتذبذب لتمنح حاملات الشحنة مزيداً من الطاقة. وهذا يعني أن عينات النحاس مع الحديد يمكن أن تعطي خلايا شمسية ذات كفاءة عالية لأن تقليل الحجم النانوي للنحاس يقلل فجوة الطاقة و يزيد الموصلية خلافاً لعينات الألمونيوم مع الحديد التي تقل فيها الموصلية.

Table of Contents

List of Tables

List of Figure

Chapter one

Introduction and Basic Concept

1. Introduction:

Materials are important in our day life physical properties of material include electric, thermal, magnetic and optical properties. The optical properties of material are useful in different application, such as domestic, medicine astronomy, manufacturing, optical property of a material is defined as it is interaction with electromagnetic variation spans the wide range from r-range with wavelength as 10-12m, through X-rays, ultraviolet visible, infrared, and family radio waves with wavelengths as a long as 10 visible light is one from electromagnetic radiation with wavelengths ranging from 0.39 to 0.77m. Light can be considered as having waves and consisting of particles called photons with a material leads to a number of phenomena. The photos may give their energy to the material (absorption) photons of identical energy immediately emitted by the material (reflection). Photons may not interact with the material structure (transmission) or during transmission photons care change in oeloeity (refraction) at any instance of light interaction with a material, the total intensity of the incident light striking a surface is equal to sum of the absorbed, reflected, and transmitted intensities [1,2]. Materials are classified on the basis of their interaction with visible light into three categories. Materials that are capable of transmitting light with relatively little absorption and reflection are called transparent materials i.e., can see through them. Translucent materials are those through with light is transmitted diffusely i.e., objects are not clearly distinguishable when viewed through those materials that are impervious to the transmission of visible light are termed as opaque materials. Material absorbs all the energy from the light photons [3, 4]. The acronym laser, constructed from light Amplification by stimulated emission of radiation, has become so common

and popular in everyday life that it is now referred to as laser. The first theoretical foundation of laser and maser was given by Einstein in 1917 using plank's law of radiation that was based on probability coefficients (Einstein coefficients) for absorption and spontaneous and stimulated emission of electromagnetic radiation. Theodor Maiman was the first to demonstrate the earliest practical laser including the first theoretical description of R.W Ladenburg on stimulated emission of electromagnetic radiation. Theodor Maiman was the first to demonstrate the earliest practical laser in 1960 after the reports by several scientists including the first theoretical description of R.W Ladenburg on stimulated emission and negative absorption in 1928 and its experimental demonstration by W.C lamb and R.C Rutherford in 1947 and the proposal of Alfred Kastler on optical pumping in 1950 and its demonstration by Brussels, Kastler and winter two years later. Maimans first laser was based on optical pumping of synthetics ruby crustal using a flash lamp that generated pulsed red laser radiation at 694 nm. Iranian scientists Javan and Bennett made the first gas laser using a mixture of He and No gases in the ration of 1:10 in the 1960. R.N Hall demonstrated the first diode laser made of gallium arsenide (Ga As) in 1962. Which emitted radiation at 850 nm, and later in the same year Nick Holon Yak developed the first semiconductor visible – light emitting laser [5, 6]. Basically, every laser system essentially has active /gain medium placed between a pair of optically parallel and highly reflecting mirrors with one of them partially transmitting and an energy source to pump active medium. The gain medium may be solid liquid or gas and have the property to amplify to the amplitude of the light wave passing through it by simulated emission while pumping may be electrical or optical. The gain medium used to place between pair of mirrors in such a way that light oscillating between mirrors passes every time through the gain medium and after attaining considerable amplification emits through the transmitting mirror. Late us consider an active medium of atoms having only two energy levels: excited level E_2 and ground level E1. If

atoms in the ground state, E_1 are excited to the upper state E_2 by means of any pumping mechanism (optical, electrical discharge, passing current or electron bombardment), then gust after few nanoseconds of their excitation, atoms return to the ground state emitting photons. According to Einstein's 1917 theory, emission process may occur in two different ways, either it may include by photo or it may occur spontaneously. The former case is termed as stimulated emission, while the laser is known as spontaneous emission. Photons emitted by stimulated emission have the same frequency, phase and state of polarization as the stimulating photo therefor they add to the wave stimulating photo on a constructive basis thereby increasing its amplitude emission to make lasing. At thermal equilibrium the probability of stimulated emission is much lower than that of spontaneous emission (1:1033) therefore most of the conventional light source are incoherent and only lasing is possible in the condition other than the thermal equilibrium [7, 8]. The optical properties is also related to some electrical properties like conductivity. Material conductivity is the ability of materials to pass an electric current in solutions the current in solutions the current is carried by cations and anions where as in mutely it is carried by electrons. How well a solution conducts electricity depends on a number of factory of ions and temperature. All substances possess some degree of conductivity in aqueous solution the level of ionic strength varies from the low conductivity of ultra-pure water to the high conductivity of concentrated chemical sample [9, 10]. The optical properties of matter can be changed by conductivity bulk matter to nanometer this can be done splitting the bulk matter into very small isolated practical's having dimensions of 1 – 300 Nanometer (1 nanometer =1 nm =10-9). Such nanomaterial's obey quantum laws [11, 12]. Nano is a popular (emerging) area of science and technology today. It has attracted the attention researchers from all walks of life, from physics to chemistry to biology and engineering. Further impetus for this movement comes from the tremendous increase in public and private funding for Nano over the

last ten years [13, 14,15]. The advantage of Nano materials comes from the fact that they obey quantum laws [16,17,18]. A prime example of this is the new National Nanotechnology Initiative (NNI) created by former president Bill Clinton. The NNI increases funding in national Nano science and nanotechnology research by hundreds of millions of dollars yearly. In addition, private sector contributions have jumped dramatically as evidenced by the plethora of small startup firms lining the tech corridors of the east west. The importance of Nano technology comes from the fact that the electrical, optical, magnetic and mechanical properties of matters can be changed and controlled with wide degrees of freedom [19, 20].

1.2 Problem Statement

The developments in semiconductor nanotechnology led to new materials having specific Properties, which can be considered for electronic applications such as diodes transistors and solar cells. These materials used in this filed in our country it is not available, very difficult synthesis and high cost. We shall search about alternative local material it has low cost, easy treatment and available.

1.3 Objectives:

Objectives are classified to general and specific objectives

1.3.1Ganeral Objectives:

The aim of this work is to synthesis Nano-material's by (Al_{2x} Fe $_{3(1-x)}$ O_4 and Cu_xFe_{1-x} O_2) formula in different molar concentration, and determination Optical, Structure and Electric properties.

1.3.2 Spicific Objectives

- To Prepare (Al_{2x} Fe $_{3(1-x)}$ O_4 and Cu_xFe_{1-x} O_2) formula in different molar concentration by sol gel method.
- To calculate optical properties and electrical conductivity such as (absorbance, absorption coefficient ect) by UV spectrometer.
- To compare the optical properties of all samples that made (Al_{2x} Fe $_{3(1-x)}$ O_4 and Cu_xFe_{1-x} O_2) formula in different molar concentration.
- To determine the structure parameter by using XRD and FTIR

.

1.4 Theses Layout

This thesis contains five chapters, chapter one included to introduction and research problems and objectives, theoretical background for topic of research and pervious study were discussed in chapter two, while chapter three included material and methods, in chapter four displayed the results and discussion of the research. Finally, chapter five contains conclusion and recommendation.

Chapter Tow
Theoretical Background and Pervious Studies

2.1 Introduction

This chapter represent of the information about the theoretical background of research and pervious study related to this work.

2.2 Nanotechnology:

Nano is the Greek word (meaning dwarf) refers to a reduction of size, or time, by 10^{-9}, which is one thousand times smaller than a micron. One nanometer (*nm*) is one billionth of a meter and it is also equivalent to ten Angstroms [21].

Nano science is a new discipline concerned with the unique properties associated with nanomaterial's, which are assemblies of atoms or molecules on a Nano scale. Nano science is actually the study of objects/particles and its phenomena at a very small scale, ranging roughly from 1 to 100 nm. "Nano" refers to a scale of size in the metric system.

Nano science is a new discipline concerned with the unique properties associated with nanomaterial's, which are assemblies of atoms or molecules on a Nano scale. Nano science is actually the study of objects/particles and its phenomena at a very small scale, ranging roughly from 1 to 100 nm. "Nano" refers to a scale of size in the metric system size range.

Nano-object: Material confine in one, two, or three dimensions at the Nano scale. This includes nanoparticles (all three dimensions in the Nano scale), Nano fiber (two dimensions in the Nano scale), and nameplates (one dimension in the Nano scale). Nano fiber are further divided into nanotubes (hollow Nano fiber) Nano rods (solid Nano fiber) and nanowire (electrically conducting or semiconducting Nano fiber) However, the term Nano-object is not very popular.

Particle: It is a minute piece of matter with definition physical boundaries. A particle can move as a unit. This general particle definition applies to Nano-objects.

Nanoparticle: It is a Nano-object with all three external dimensions in the Nano scale. Nanoparticles can have amorphous or crystalline form and their surfaces can act as carriers for liquid droplets or gases.

Nano particulate matter: It refers to a collection of nanoparticles, emphasizing their collective behavior.

Agglomerate: It is a group of particles held together by weak forces such as van der Waals forces, some electrostatic forces, and surface tension. It should be noted that agglomerate will usually retain a high surface-to-volume ratio.

Aggregate: It is a group of particles held together by strong forces such as those associated with covalent or metallic bonds. It should be noted that an aggregate may retain a high surface-to-volume ratio.

Nanotechnology is the construction and use of functional structures designed from atomic or molecular scale with at least one characteristic dimension measured in nanometers. Their size allows them to exhibit novel and significantly improved physical, chemical, and biological properties, phenomena, and processes because of their size. Thus, nanotechnology can be definition as research and development that involves measuring and manipulating matter at the atomic, molecular, and supramolecular levels at scales measured in approximately 1–100 nm in at least one dimension. When characteristic structural features are intermediate between isolated atoms and bulk materials in the range of approximately 1–100 nm, the objects often display physical attributes substantially different from those displayed by either atoms or bulk materials. The term “nanotechnology” is by and large used as a reference for both Nano science and nanotechnology especially in the public domain. We should distinguish between Nano science and nanotechnology. Nano science is a convergence of physics, chemistry, materials science, and biology, which deals

with the manipulation and characterization of matter on length scales between the molecular and the micron size. Nanotechnology is an emerging engineering discipline that applies methods from Nano science to create products [22].

Nano-coatings. Applications of Nano-coatings are used to stabilize highly explosive materials, making it much safer to handle nuclear and other warheads. Nano-coatings can also stabilize biological and chemical agents, making them longer lasting and diversifying their means of delivery. Radio-frequency shield coatings could provide privacy and security to shield buildings and wireless networks from radio waves.

Nano-optics. Nano-engineered negative index met materials are moving stealth technology toward cloaking and invisibility, based on their ability to deflect light away from around an object rather than reflect it. Optical fibers married with nanowires portend the advent of solar-rechargeable, portable and wearable electronic devices [23].

2.3 Iron Oxide

Nano particles of magnetic oxides have attracted great interest because of their unique physical properties. There are two crystal types of Fe_2O_3 which are the magnetite and hematite. Since they are widely used in preparation of recording materials, pigments, catalysts, sorbent for removal of heavy metals from water and soil and gas sensitive materials, Nano crystalline iron oxide have been of considerable importance in recent years. Iron oxide is synthesized using different techniques. These are precipitation, sol-gel, combustion processes, micoemulism and electrochemical processes. Unfortunately, these methods need expensive organic products the solid-state chemical reaction method looks cheaper and ecologically clean [18].

2.4 Aluminum Oxide (Al_2O_3)

Aluminum, the second most abundant metal in the earth's crust, exhibits only the trivalent state in the compound and in solution [24]. Metal oxides are widely

used in adsorption technology as adsorbent surfaces because of their efficiency, low cost and unique physical properties. One of the renowned oxides is Aluminum oxide (Al_2O_3) which is an amphoteric oxide known as alumina and found in many crystalline structures like 'α-Al_2O_3, γ- Al_2O_3, θ- Al_2O_3, η- Al_2O_3' etc. Aluminum oxide is characterized by its non-toxic, easy used, chemical stability and has many hydroxide groups all these properties mad it efficient adsorbent. From 1923 Aluminum oxide had usage as adsorbed to remove Pigments, antibiotics, heavy metals, dissolved organics etc. In the light of the continuous development in the field of nanotechnology and its use in treatment pollution of the environment, interest increasing in the use of metal oxides as nanoparticles as absorbers to remove pollutants from the environment, especially Aluminum oxide nanoparticles inasmuch to it inexpensive, high surface area, surface reactivity, well adsorption ability, surface acidity and thermal stability [19]. Nanostructured aluminum oxide is the most important metal oxide material which is used widely in many industrial applications, such as catalyst, surface passivation, ant-reflection coating, sensors, gas diffusion barrier, abrasive materials and Nano laminates. Al_2O_3 is a wide band-gap (6 eV at 300 k for bulk material) dielectric material which can exist in different crystalline forms such as gamma, delta, theta and alpha phases. There are many techniques to prepared aluminum oxide nanoparticles powder including ball milling, hydrothermal, sol-gel, co-precipitation, pyrolysis, laser ablation, vapor phase reaction and combustion methods [20].

2.5 Crystal Structure

As noted above high performance semiconductor devices are based on crystalline materials. Crystals are periodic structures made up of identical building blocks. While in “natural” crystals the crystalline symmetry is fixed by nature, new advances in crystal growth techniques are allowing scientists to produce artificial crystals with modified crystalline structure. These advances

depend upon being able to place atomic layers with exact precision and control during growth, leading to “low dimensional systems”. To define the crystal structure, two important concepts are introduced. The lattice represents a set of points in space forming a periodic structure. The lattice is by itself a mathematical abstraction. A building block of atoms called the basis is then attached to each lattice point yielding the physical crystal structure. To define a lattice, one defines three vectors a1, a2, a3, such that any lattice point R_ can be obtained from any other lattice point R by a translation [24].

$$R\_=R+m_1a_1+m_2a_2+m_3a_3 \quad (2.1)$$

where m_1, m_2, m_3 are integers. Such a lattice is called a Bravais lattice. The crystalline structure is now produced by attaching the basis to each of these lattice points.

Lattice + basis = crystal structure

The translation vectors a1, a2, and a3 are called primitive if the volume of the cell formed by them is the smallest possible. There is no unique way to choose the primitive vectors. It is possible to define more than one set of primitive vectors for a given lattice, and often the choice depends upon convenience. The volume cell enclosed by the primitive vectors is called the Primitive unit cell. Because of the periodicity of a lattice, it is useful to define the symmetry of the structure. The symmetry is defined via a set of point group operations which involve a set of operations applied around a point. The operations involve rotation, reflection and inversion. The symmetry plays a very important role in the electronic properties of the crystals. For example, the inversion symmetry is extremely important and many physical properties of semiconductors are tied to the absence of this symmetry. As will be clear later, in the diamond structure (Si, Ge, C, etc.), inversion symmetry is present, while in the Zinc Blende structure (GaAs, AlAs, InAs, etc.), it is absent. Because of this lack of inversion symmetry, these semiconductors are piezoelectric, i.e., when they are strained an electric potential is developed across the opposite faces of the crystal. In crystals

with inversion symmetry, where the two faces are identical, this is not possible [25].

The size of the unit cell and the arrangement of atoms in a crystal may be determined from measurements of the diffraction of X-rays by the crystal,

2.6 Simple Lattices:

Although no semiconductors crystallize into simple lattice, they form the basis for understanding the more complicated semiconductor's structure. We will use them to illustrate some of the more important concepts involved in forming a mathematical description of the crystal lattice.

A concept most useful in specifying the underlying geometry of crystal structure is the Bravais Lattice. A Baravais lattice is the infinite matrix of points which, together with the atoms or molecules situated at the points, form the crystal structure it has the property that arrangement of Lattice sites around any given lattice site is the same as that around any other site mathematically, A Bravais Lattice consist of all poivrts generated by the vectors.

$$R= \sum n_i, a_i \quad i= 1,2,3 \qquad (2.2)$$

Where a_i is noncoplanar vectors and n_i take on all integral values. The a_i which generate the Bravais Lattice is know as primitive vectors.

In the simple cubic structure, which has an atom at each corner of a cube of dimension the Bravais Lattice can be determined by three mutually orthogonal vectors.

a_1=ax, a_2 =ay, a_3=az

where x, y, and z are Cartesian unit vectors. This set of vectors demonstrates the basic symmetry of the structure and it is easy to see that the entire Bravais Lattice can be constructed with these vectors this set of primitive vectors is not unique, however, in defining the simple cubic Brava's can also be used to construct the Lattice as well as an infinite number of other sets.

The boy. centrated cubic structure has an atom at each corner of cubic dimension and one at the point determined by the intersection of the cubic body diagonals, another Lattice of interest in semiconductor crystal structure is the hexagonal close packed Lattice. Although not a Baravais Lattice, because the Lattice sites are not equivalent it consists of two interpenetrating simple hexagonal Lattices which are Bravais Lattice. The simple hexagonal Lattice consist of Lattice site at each corn of an equilateral triangle of side a, with an additional set of points on triangle at a distance above the first.[25]

2.7 X-ray Powder Diffraction (XRD):

X-ray diffractometers consist of three basic elements: an X-ray tube, a sample holder, and an X-ray detector. X-rays are generated in a cathode ray tube by heating a filament to produce electrons, accelerating the electrons toward a target by applying a voltage, and bombarding the target material with electrons. When electrons have sufficient energy to dislodge inner shell electrons of the target material, characteristic X-ray spectra are produced. These spectra consist of several components, the most common being Kα and Kβ. Kα consists, in part, of Kα1 and Kα2. Kα1 has a slightly shorter wavelength and twice the intensity as Kα2. The specific wavelengths are characteristic of the target material (Cu, Fe, Mo, and Cr). Filtering, by foils or crystal monochrometers, is required to produce monochromatic X-rays needed .for diffraction. Kα1and Kα2 are sufficiently close in wavelength such that a weighted average of the two is used. Copper is the most common target material for single-crystal diffraction, with CuKα radiation = 1.5418Å. These X-rays are collimated and directed onto the sample. As the sample and detector are rotated, the intensity of the reflected X-rays is recorded. When the geometry of the incident X-rays impinging the sample satisfies the Bragg Equation, constructive interference occurs and a peak in intensity occurs. A detector records and processes this X-ray signal and converts the signal to a count rate which is then output to a device such as a

printer or computer monitor. The geometry of an X-ray diffractometer is such that the sample rotates in the path of the collimated X-ray beam at an angle θ while the X-ray detector is mounted on an arm to collect the diffracted X-rays and rotates at an angle of 2θ. The instrument used to maintain the angle and rotate the sample is termed a goniometer. [26]

In powder x-ray diffraction, the sample consists of many small crystallites which are assumed to be randomly oriented. This produces rings of diffracted x-rays, defined by the angle between the incident and diffracted beams, 2θ. The diffraction condition is determined by the atomic unit cell. In this way, the structure type of a material and unit cell size can easily be determined. If more than one type of material is present, the diffraction pattern will be a superposition of each of the components. If only phase identification is desired, this often provides enough information. Reference [27] gives a good example of how this is done. The intensities of each diffraction line is determined by the atomic constituents, and their placement in the unit cell. In principle, both of these can be determined from the intensities. In practice, this is difficult to achieve. A primary concern is texturing, or preferred orientation of the crystallites. If the crystallites are plate or needle like, they will tend to lay in the sample holder in a non-random orientation. This will cause a variation in the intensities. Also, individual diffraction peaks often overlap one another in a powder pattern. Since the determination of the structure depends on how much intensity is associated with each peak, having overlapping peaks complicates the solution process. It is often easiest to do structural analyses on single crystal samples. Powder diffraction sample holders are usually for flat, planar samples. If the incident angle of the incoming x-rays with respect to the sample plane is equal that of the diffracted beam being detected, the x-ray beam is partially focused (Bragg-Botano parafocusing) to give a narrower diffraction peak. For this reason, the sample plane is usually rotated (by an angle $\omega = \theta$) as the detector rotates (by angle 2θ).

In Fig.2-1 shows the setup of the x-ray diffractometer. The produced x-ray from the tube is filtered to produce monochromatic radiation, collimated and then hit the specimen at position C. The x-rays diffracted by the specimen are focused through a slit F onto the detector during rotation of the detector on the diffractometer circle through an angle 2θ. The counted intensity is proportional to the number of x-rays of a particular energy, which in turn represents the number of crystal planes. The angle 2θ represents the plan position and its direction. According to Bragg's law: $2\, d_{hkl} \sin\theta = n\, \lambda$, where, n is an integer, λ is the wavelength of incident wave, d is the spacing between the planes in the atomic lattice, (hkl) is Miller index of the scattering plane and θ is the angle between the incident ray and the scattering planes. [28]

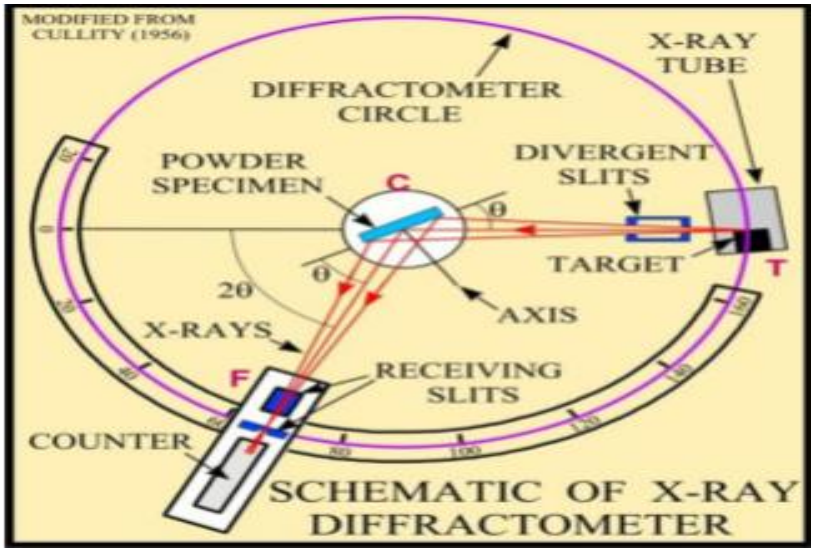

Figure (2.1): X-ray diffractometer

Bragg presented a simple explanation of the X-rays diffraction in crystals assuming that the incident waves are reflected secularly by parallel planes of atoms in the interior of the crystal, being that each plane reflects only a small

fraction of the radiation and that diffraction beams are formed only when the reflection angle with respect to the parallel planes (that are separated from each other by an interplanar distance *d*) satisfies the following relation (called Bragg law and illustrated in Fig (2.1).

$$2d_{hkl}\sin\theta = n\lambda \tag{2.3}$$

When n represents the order of the reflection. And the separation distance is

Taken to be $$d_{hkl} = 1/|H_{hkl}| \tag{2.4}$$

Where (h, k and l) are miller indices, $\vec{H}_{hkl} = h\vec{a}^* + k\vec{b}^* + l\vec{c}^*$ is diffraction factor, $\vec{a}^* = 2\lambda\frac{\vec{b}\times\vec{c}}{v}$, $\vec{a}^* = 2\lambda\frac{\vec{b}\times\vec{c}}{v}$, $\vec{a}^* = 2\lambda\frac{\vec{b}\times\vec{c}}{v}$ are reciprocal vectors, and $V = \vec{a}.(\vec{b}\times\vec{c})$

Is volume of unit cell.

Since x-rays have wavelength which is about the same size as atomic spacing in a solid crystal; the crystal might serve as a three-dimensional diffraction grating for x-rays.

Bragg suggested that the phenomenon of diffraction could by pictured as a reflection of the incident beam from lattice planes. Consequently he derived a mathematical expression for the reflection condition.

At a glancing angle θ , each plane must be pictured as reflecting , a fraction of the incident beam . the reflected rays then combine to form a constructive interference beam , if they differ in phase by whole number of wavelengths , that is :

The path difference $= n\lambda$ where n= 1,2,3, …

AB=d sin θ and BC = d sin θ (2.5)

Therefore, the path difference = AB+BC $= n\lambda$

$$n\lambda = 2d\sin\theta \tag{2.6}$$

This is Bragg s law which determines the angle at which diffraction maxima occurs. This condition for reflection has a number of solutions for θ for particular values of d and λ [32].

$$\theta = \sin^{-1}\left(\frac{n}{2d}.\lambda\right), \sin^{-1}\left(\frac{n}{2d}.2\lambda\right), ...etc \qquad (2.7)$$

These statements mply that for a given experimental arrangement with monochromatic radiation (single λ) , a set of planes is rotated through certain position where the phase difference are $\lambda, 2\lambda, 3\lambda \ldots$ then a series of reflections will occur , since the argument of $\theta = \sin^{-1}\left(\frac{n\lambda}{2d}\right)$ can never exceed unity , then the maximum phase difference $n\lambda$ will be equal to 2d. therefore this condition gives the maximum number of reflections that can emanate from a crystal . of course a crystal possesses an infinite number of sets of planes and from equation (2.7)

This may represent infinite different values of d. However since the only possible reflections are those for which $\frac{n\lambda}{2d} \leq 1$

Then it is clear that only planes for which $d \geq \frac{\lambda}{2}$ can reflect [29]. The lattice points forming a space lattice in a crystal may be thought of as occupying various sets of parallel planes .Each plane has a particular orientation. In order to satisfy the orientation, one employs the so called miller indices; these are defined as the inverse of the position of the atoms in the crystal axes and they are represented in a form such as (hkl). When the indices are shown enclosed by brackets, such as [hkl] they refer to equivalent crystal plane, even though their miller indices may differ.

We may note here that the miller indices of a set of planes are related to the cosine of the normal to these planes .For a cubic crystal , $\frac{1}{h}, \frac{1}{k}, \frac{1}{l}$ are intercept of

the plane (hkl) on a_1,a_2,a_3 axes respectively , so that the equation of the plane may be written as :

$$\frac{a_1}{1/h}, \frac{a_2}{1/k}, \frac{a_3}{1/l} = 1 \qquad \text{or} \quad a_1 h + a_2 k + a_3 l = 1 \tag{2.8}$$

Where a_1, a_2 and a_3 are the crystal axes.

The separation between two parallel planes (d) for a cubic crystal is given by:

$$d = \frac{a}{\sqrt{\left(h^2 + k^2 + l^2\right)}} \tag{2.9}$$

For the determination of the (hkl) planes of a sample that have an orthorhombic unit cell a general relation can be derived by using bragg s condition. Then the indexing can be done according to the following:

From the relation that describes the separation of the parallel planes, we have:

$$d_{hkkl} = x\cos\alpha = y\cos\beta = z\cos\gamma \tag{2.10}$$

Also, we have:

$$\cos^2\alpha + \cos^2\beta + \cos^2\gamma = 1 \tag{2.11}$$

From equation (2.10) and (2.11) we obtain:

$$d_{hkl} = \frac{1}{\left(\frac{1}{x^2} + \frac{1}{y^2} + \frac{1}{z^2}\right)^{1/2}} \tag{2.12}$$

By using the relation between the axis and miller indices, we get:

$$h = \frac{na}{x}, k = \frac{nb}{y}, l = \frac{nc}{z} \tag{2.13}$$

By substituting equation (2-13) in equation (2-12)

$$d_{hkll} = \frac{n}{\sqrt{\frac{h^2}{a^2} + \frac{k^2}{b^2} + \frac{l^2}{c^2}}} \tag{2.14}$$

$$\frac{1}{d_{hkl}} = \frac{h^2}{a^2} + \frac{k^2}{b^2} + \frac{l^2}{c^2} \tag{2.15}$$

The lattice parameters in orthorhombic structure: $a \neq b \neq c$.

Then using Bragg condition where: $n\lambda = 2d\sin\theta$ and substituting with equation (2.15)

We obtain:

$$n\lambda = \frac{2n\sin\theta}{\sqrt{\frac{h^2}{a^2}+\frac{k^2}{b^2}+\frac{l^2}{c^2}}} \tag{2.16}$$

Equating the two sides

$$\lambda^2 = \frac{4\sin^2\theta}{\left(\frac{h^2}{a^2}+\frac{k^2}{b^2}+\frac{l^2}{c^2}\right)} \tag{2.17}$$

Thus:

$$\left(\frac{h^2}{a^2}+\frac{k^2}{b^2}+\frac{l^2}{c^2}\right) = \frac{4\sin^2\theta}{\lambda^2} \tag{2.18}$$

Here, λ is the wave length of Cu K_α radiation that was used in the experiment where,

λ=1.54060 A° substituting this value of λ in equation we get:

$$\left(\frac{h^2}{a^2}+\frac{k^2}{b^2}+\frac{l^2}{c^2}\right) \cong 1.68531\sin^2\theta \tag{2.19}$$

Equation (2.18) can be considered as general relation that can be applied for samples which have orthorhombic unit cell structures in order to get the values of miller indices (hkl).

2.8 Fourier Transport Infrared Spectroscopy (FTIR)

Infrared (IR) spectroscopy is a one-photon effect and the photon absorption results in a vibrational motion of a molecule. Infrared spectra originate from the vibrational motions of atoms in chemical bonds within the molecular structure. When a beam of light containing the (IR) radiation interacts with a sample [27]. Fourier spectroscopy" is a general term that describes the analysis of any varying signal into its constituent frequency components, Fourier Transform Infrared Spectroscopy (FTIR) is a reliable method of infrared spectroscopy and offers several analytical opportunities in academic, analytical and forensic labs,

FT-IR spectroscopy includes the absorption, reflection, emission, or photo acoustic spectrum obtained by Fourier transform of an optical interferogram [28,29,30]. The infrared region (10-14000 cm-1) of the electromagnetic spectrum is divided into three regions: the near-, mid-, and far-IR. The mid-IR (400-4000 cm-1) is the most commonly used region for analysis as all molecules possess characteristic absorbance frequencies and primary molecular vibrations in this range. Mid-infrared spectroscopy . Methods are based on studying the interaction of infrared radiation with samples. As IR radiation is passed through a sample, specific wavelengths are absorbed causing the chemical bonds in the material to undergo vibrations such as stretching, contracting, and bending. Functional groups present in a molecule tend to absorb IR radiation in the same wavenumber range regardless of other structures in the molecule, and spectral peaks are derived from the absorption of bond vibrational energy changes in the IR region. Thus, there is a correlation between IR band positions and chemical structures in the molecule. In addition to providing qualitative information about functional groups, IR spectra can provide quantitative information, such as the concentration of bacteria in a growth medium. An IR spectrum is measured by calculating the intensity of the IR radiation before and after it passes through a Sample and the spectrum is traditionally plotted with Y-axis units as absorbance or transmittance and the X- axis as wave number units. For quantitative purposes it is necessary to plot the spectrum in absorbance units [31, 32]. FT-IR absorbance spectra follow Beer‘s law, which relates concentration to absorbance as in Eq. (2.19)

$$A_\lambda = L\ \varepsilon_\lambda C \qquad (2.20)$$

Where A_λ_= Absorbance, L = Path length, ε_λ = Absorptivity, c = Concentration

Transmittance is not directly proportional to the concentration and is defined in Eq. (3.2)

$$T\% = \frac{IS}{IR} \qquad (2.21)$$

Where I_S = Intensity of IR beam after passing through the sample, I_R = Intensity of IR beam before passing through the sample, T= Transmittance

2.9 Spectroscopy

In principle, a spectrometer is the simplest of scientific instruments. The term spectroscope derives from two root words: the Latin word spectrum, meaning image, and the Greek word skopein, to view, (e.g., microscope, telescope, etc.). So, a spectroscope is an instrument that permits visual observation of spectra. Instruments that record a spectral image on a photographic plate (the spectroscope plus the tube plate holder) are commonly called spectrographs. A spectroscope can thus "fingerprint" a material by disclosing what elements the material contains and in what proportions. In certain cases, it is not even necessary to touch the object being studied. Almost anything that emits, absorbs, or reflects light Not only can elements be identified (the method is called spectrochemical or elemental analysis), but information can also be obtained on the constituents of the elements — the electrons and atomic nuclei—as well as the atoms and molecules themselves. This aspect is sometimes referred to as atomic or molecular spectroscopy. Spectroscopy has been the means whereby physicists and chemists have learned most of what they now know about the nature of matter. It was originally limited to visible light, but new ways of generating and detecting other kinds of energy are constantly being developed. These are quickly. [30]. There are many types of spectroscopy and they are used to detect, identify and quantify data about material samples as gases, liquids and solids. As such, spectroscopy is used to determine both the chemical composition as well as measure the physical properties of matt etc. UV-Vis spectroscopy is an analytical technique that measures the number of discrete wavelengths of UV or visible light that are absorbed by or transmitted through a sample in comparison to a reference or blank sample. This property is influenced by the sample composition, potentially providing information on what is in the sample and at what concentration. Since this spectroscopy

technique relies on the use of light, let's first consider the properties of light. Light has a certain amount of energy which is inversely proportional to its wavelength. Thus, shorter wavelengths of light carry more energy and longer wavelengths carry less energy. A specific amount of energy is needed to promote electrons in a substance to a higher energy state which we can detect as absorption. Electrons in different bonding environments in a substance require a different specific amount of energy to promote the electrons to a higher energy state. This is why the absorption of light occurs for different wavelengths in different substances. Humans are able to see a spectrum of visible light, from approximately 380 nm, which we see as violet, to 780 nm, which we see as red.[1] UV light has wavelengths shorter than that of visible light to approximately 100 nm. Therefore, light can be described by its wavelength, which can be useful in UV-ViS spectroscopy to analyze or identify different substances by locating the specific wavelengths corresponding to maximum absorbance [30]

2.9.1 Ultraviolet -Visible Spectroscopy (UV-VIS)

Ultraviolet and Visible Spectroscopy is absorption spectroscopy uses electromagnetic radiations between 190 nm to 800 nm and is divided into the ultraviolet (UV, 190-400 nm) and visible (VIS, 400-800 nm) regions. Since the absorption of ultraviolet or visible radiation by a molecule leads transition among electronic energy levels of the molecule, it is also often called as electronic spectroscopy [31]. When radiation interacts with matter, a number of processes can occur, including reflection, scattering, absorbance, Fluorescence/phosphorescence (absorption and reemission), and photochemical reaction (absorbance and bond breaking). In general, when measuring UV-visible spectra, we want only absorbance to occur. Because light is a form of energy, absorption of light by matter causes the energy content of the molecules (or atoms) to increase. The total potential energy of a molecule generally is represented as the sum of its electronic, vibrational, and rotational energies [32].

In the UV-Vis spectral range transitions between electronic energy levels can be observed, which determine the absorption bands in the UV-Vis region. An electron is excited when the frequency of the incident electromagnetic radiation is the same as the difference of energy between two electronic states. This difference of energy depends on the electronic structure of the molecule and of its "environment". For a transition to happen after absorption of radiation it is necessary to have a dislocation of charge and some rules [25].

2.9.2 Optical Properties

Optical methods are very useful for the quantitative determination of the electronic band structure of Martials. In this study optical absorbance, reflectivity, transmission and refraction provide the way to determine the dielectric constant of the normal human blood sample, which is related to the band structure. The dielectric constant is related to the optical conductivity. The term "optical conductivity" means the electrical conductivity in the presence of an alternating electric field [25]

2.9.3 Absorption

The intensity of the net absorbed radiation is dependent on the character of the medium as well as the path length within. The intensity of transmitted or non-absorbed radiation continuously decreases with distance x that the light traverses:

$$I_T = I_o e^{-\beta x} \tag{2.22}$$

Where is the intensity of the non-reflected incident radiation and ß the absorption Coefficient (in mm^{-1}), is characteristic of the particular material; furthermore, varies with wavelength of the incident radiation. The distance parameter x is measured from the incident surface into the material. Materials that have large values are considered highly absorptive [25]

2.9.4 Transmission

The phenomena of absorption, reflection, and transmission may be applied to the passage of light through a transparent solid. For an incident beam of intensity I0 that impinges on the front surface of a specimen of thickness l and absorption coefficient, the transmitted intensity at the back face IT is

$$I_T = I_o(\,1 - R)^2 e^{-\beta l} \tag{2.23}$$

Where R is the reflectance; for this expression, it is assumed that the same medium exists outside both front and back faces. The derivation of Equation (2.8) is left as a homework problem. Thus, the fraction of incident light that is transmitted through a transparent material depends on the losses that are incurred by absorption and reflection. Again, the sum of the reflectivity R, absorptivity A, and transmissivity T, is unity according to Equation (2.2). Also, each of the variable's R, A, and T depends on light wavelength. This is demonstrated the transmission [23].

2.9.5 Reflection

When light radiation passes from one medium into another having a different index of refraction, some of the light is scattered at the interface between the two media even if both are transparent. The reflectivity R represents the fraction of the incident light that is reflected at the interface, or

$$R = \frac{I_R}{I_o} \tag{2.24}$$

Where I0 and IR are the intensities of the incident and reflected beams, respectively. If the light is normal (or perpendicular) to the interface, then

$$R = \left(\frac{n_2 - n_1}{n_{2+} n_1}\right)^2 \tag{2.25}$$

Where n1 and n2 are the indices of refraction of the two media. If the incident light is not normal to the interface, R will depend on the angle of incidence. When light is transmitted from a vacuum or air into a solid s, then

$$R = (\frac{n_s - 1}{n_s + 1})^2 \quad (2.26)$$

because the index of refraction of air is very nearly unity. Thus, the higher the index of refraction of the solid, the greater the reflectivity [23]

2.9.6 Absorption coefficients

Much of the information about the properties of materials is obtained when they interact with electromagnetic radiation. When a beam of light (photons) is incident on a material, the intensity is expressed by the Lambert-Beer- law as Equation (2.3). If this condition for absorption is met, it appears that the optical intensity of the light wave, (I), is exponentially reduced while traveling through the film. If the power that is coupled into the film is denoted by I0, gives the transmitted intensity that leaves the film of thickness d.(α) Is called "absorption coefficient". From Equation (2.8) it follows that

$$\alpha = -\frac{1}{d}\, Lin(\frac{I}{I_o}) \quad (2.27)$$

It is clear that α must be a strong function of the energy hν of the photons. For hν < Eg (direct), no electron hole pairs can be created, the material is transparent and α is small. For hν ≥ Eg (direct), absorption should be strong. All mechanisms other than the fundamental absorption may add complications (e.g., "sub band gap absorption" through exactions), but usually are not very pronounced. Optical transmission measurements were carried out to determine the film thickness, the wavelength dependence of the refractive index and optical absorption coefficient. The optical constants were determined from the optical transmission measurements using the method described by Swanepoel [23]

The transparent substrate has a thickness several orders of magnitude larger than (d) and has index of refraction (n) and absorption coefficient (α = 0). The index of refraction for air is taken to be n0 =1. In the transparent region (α =0) the transmission is determined by n and s through multiple reflections. In the region of weak absorption α is small and the transmission begins to decrease. In the medium absorption region α is large and the transmission decreases mainly due to the effect of α. In the region of strong absorption, the transmission decreases drastically due almost exclusively to the influence of α. If the thickness d is uniform, interference effects give rise to the spectrum [30].

2.9.7 Refractive index

Light that is transmitted into the interior of transparent materials experiences a decrease in velocity, and, as a result, is bent at the interface; this phenomenon is termed refraction. The index of refraction n of a material is defined as the ratio of the velocity in a vacuum c to the velocity in the medium or

$$n = \frac{c}{v} \tag{2.28}$$

The magnitude of n (or the degree of bending) will depend on the wavelength of the light. This effect is graphically demonstrated by the familiar dispersion or se parathion of a beam of white light into its component colors by a glass prism. Each color is deflected by a different amount as it passes into and out of the glass, which results in the separation of the colors. Not only does the index of refraction affect the optical path of light, but also, as explained shortly, it influences the fraction of incident light that is reflected at the surface. Just as Equation (2.13) defines the magnitude of c, an equivalent expression gives the velocity of light in a medium as

$$v = \frac{1}{\sqrt{c\mu}} \tag{2.29}$$

the permittivity and permeability of the particular substance. From Equation (2.14), we have

$$n = \frac{c}{v} = \frac{\sqrt{\epsilon\mu}}{\sqrt{\epsilon_o \mu_o}} = \sqrt{\epsilon_r \, \mu_r} \tag{2.30}$$

Where μ_r and ε_r are the dielectric constant and the relative magnetic permeability, respectively. Because most substances are only slightly magnetic, and

$$n \cong \sqrt{\epsilon_r} \tag{2.31}$$

Thus, for transparent materials, there is a relation between the index of refraction and the dielectric constant [8].

2.10 Preparation of Nanoparticles

Synthesis of nonmetal and metal oxide (MO) materials involves substantial synthetic ingenuity. Although one can develop a balanced method to the synthesis of nanomaterials, there is continually an element of serendipity. A verity of nanomaterial's has been synthesized in the last several decades by the old-style ceramic method, which includes mixing and crushing powders of the constituent oxides, carbonates, and other compounds and heating them at elevated temperatures with transitional grinding when necessary. Some of the important chemical methods of synthesis of oxides are precipitation and precursor methods, ion exchange and sol-gel technique, top chemical methods, hydrothermal/solvothermal approaches, combustion technique (self-propagating high- and low-temperature method and solution combustion method), microwave-assisted and liquid-liquid interface method, etc. Some of them have been briefly described in the following sections [22]

2.10.1 Sol Gel Method

A sol-gel is a colloidal suspension of solid particles in liquid. In sol gel process, the precursors (starting compound) for preparation of a colloid consist of metal or metalloid element surrounded ligands common precursors for Aluminum oxide include inorganic (containing no carbon) salts such as AL $(NO_3)_3$ and organic compound such as AL $(OC_4 H_9)_3$ Transition metal oxide gels include one of the most successful sol-gel products. Transition metal oxide gels are also the basis of several important thin –film ferroelectric such as Barium titan ate as well as semiconducting $V_2 O_5$ films, electro chromic W_3 O films, or particles. Recently transition metal oxide gels have been used extensively in chemical routes to high- temperature superconducting ceramic. Sol-gel methods have been recognized as interesting procedures to prepare catalysts. The versatility of the sol-gel techniques allows control of the texture, composition, homogeneity and structural properties of solids, and makes possible production of tailored materials such as dispersed metals, oxide catalysts and chemically modified supports. The sol-gel process has emerged as a standard production technique for engineering materials. Unlike the more conventional methods, the sol-gel technique allows for preparing porous materials in a “one-pot” with a homogeneous distribution of components on the atomic scale through a technology of low temperature synthesis and with full control of the finite product microstructure. The sol-gel chemistry involves two distinct phases: solution and gelation: a sol is a colloidal suspension of solid particles, whereas a gel is an interconnected network of solid phase particles that form a continuous entity throughout a secondary, usually liquid, phase. The advantages of sol-gel methods include: high yield, low operation temperatures, and low production costs. Even more, the sol-gel synthesis resulted in possessing unique features, namely the possibility of control over the physic–chemical properties of the resulting compounds through a careful variation of the parameters affecting the

various synthesis steps. The sol-gel process is generally considered as “soft chemistry” in contrast to more classical industrial techniques for glass and ceramic manufacturing, which require very high temperatures. Nowadays, the term ‘sol-gel’ is used more broadly as covering the synthesis of solid materials, such as metal oxides, from solution-state precursors. The development of technologically advanced synthesis routes that overcome the obstacles that are encountered in the most traditional procedures allowed the sol-gel technique to become a unique tool in the design of metal oxides with controlled architecture.

2.11 Conductivity

How superconductivity emerges from a strongly correlated normal state is one of the most important problems in the field of strongly correlated electron systems. One of the most powerful bulk probes of carrier dynamics is the optical conductivity. For example, the changes of the integral of the optical conductivity upon superfluid condensation [45,46] can be linked to the kinetic energy change, and therefore gives a direct probe of the origin of the condensation energy. Much effort was recently devoted to measure this kinetic energy difference between normal and superconducting state [3,5] using a sum rule, by integrating careful measurements of the optical conductivity up to large enough cutoff of the order of 1 eV in both normal and superconducting state. It has been shown that in the over doped regime, the absolute value of the kinetic energy decreases, while in the under doped regime the system gains kinetic energy. These surprising experimental results have been the subject of lively controversy but have by now been obtained by at least three experimental groups. It is well known that the approach to a Mott transition causes a dramatic reduction of the low energy spectral optical weight. In this paper we address the more refined issue of how the difference between the optical conductivity in the normal and superconducting state, and the consequent difference in kinetic energy are affected by the proximity to the Mott transition.

2.11.1 Optical Conductivity

The optical conductivity of an electronic model governed by a Hamiltonian H consisting of a band with dispersion ε_k and gauge invariant interaction terms obeys the f-sum rule [26]

$$\int_0^\infty \acute{\delta}(x)d(x) = -\frac{\pi e^2}{4}\langle T\rangle \tag{2.32}$$

The conductivity $\grave{\delta}$ is given by the current-current correlation function obtained by Peierls substitution coupling a vector potential A to the Hamiltonian H = (j =δH / δA , T = δ^2H / δA^2) and the bracket $\langle..|..\rangle$ denotes the thermal average with respect to H. T is given by

$T = -\sum_{k,\delta,\alpha=(x,y)}[\frac{d^2\,\varepsilon_k}{dk^2}]n_{k\alpha}$. In the Hubbard model nk is the electron momentum distribution function while in the t-J model nk is the momentum distribution of the electron operator projected to the subspace without the double occupancy. For model lattice Hamiltonians with nearest neighbor hopping, T is the kinetic energy operator. The experimental inference of $\langle T\rangle_{super} - \langle T\rangle_{normal}$ is therefore extremely important for understanding the mechanism of high temperature superconductivity. Here $\langle T\rangle_{super}$ and $\langle T\rangle_{normal}$ are kinetic energy in superconducting and normal state, respectively. Notice that this quantity requires the evaluation of $\langle T\rangle_{normal}$ below the superconducting transition, a quantity which is well defined and can be calculated only in a mean field framework. Only mean field theory provides the possibility of defining the continuation of the normal state below Tc. This is the procedure done in BCS theory, and our approach represent the extensions of these ideas to correlated systems. Experimentally it is estimated by an extrapolation procedure from the normal state data as described in references, which necessarily involves additional approximations. In the Hubbard model, the optical conductivity has two contributions: a low energy contribution due to a motion of holes and a high

energy feature at an energy scale of order U due to transitions to the upper Hubbard band involving doubly occupied sites. Hence the operator on the right hand side of eq. (2.19) is the sum of the two different contributions which cannot be separate. It can be found that entering the superconducting state results in a reduction of kinetic energy of the Hubbard model, in stark contrast with the BCS theory where the kinetic energy increases upon entering the superconducting state. The reduction of the kinetic energy was also found in the t-J model treated within the separately approximation .Here we use the t-J model to evaluate separately the two physically different contributions, motion of holes and super exchange contribution. This allows us to make direct contact with optical experiments which measure the kinetic energy of the holes since the cutoffs which are used are such that the transitions into the upper Hubbard band, or the inter band transitions, are not included. We use the Cluster Dynamical Mean Field method on a plaquette. This approach has been used by several groups to elucidate several qualitative aspects of the physics of the cuprates such as their phase diagram and the variation of the spectral function and the electron lifetime along the Fermi surface .We will show that this approach clearly captures the striking feature that doping induces a sign change of the difference between normal state and the superconducting state kinetic energy.

2.11.2 Electrical Conductivity

The electrical conductivity of foods is of relatively recent interest to researchers. Little literature exists on this topic, since electrical conductivity was not critical in food applications prior to the late 1980s. Recent attention on electrical resistance heating of foods and pulsed electrical field in pasteurizing foods has necessitated the need for information on the electrical conductivity of foods. Electrical conductivity is a critical parameter for both the Ohmic heating and pulsed electrical field processes. Knowledge of a food's electrical conductivity while under Ohmic heating or pulsed electrical field conditions is essential for

process design. Electrical conductivity is the reciprocal of resistance through a unit cross-sectional area A over a unit distance L, or the reciprocal of resistivity.

$$\sigma = (\frac{L}{AR}) \tag{2.33}$$

or

$$\sigma = \left(\frac{I}{V}\right)\left(\frac{L}{A}\right) \tag{2.34}$$

where, A is the area of cross section of the sample (m^2), I is the current through the sample (A), L is the electrode gap or length of sample (m), R is the resistance of the sample (Ω), V is the voltage across the sample (V), and σ is the specific electrical conductivity (S/m). The definition above has been used to design experiments for measuring the electrical conductivity of foods. Standard methods and commercial conductivity meters are available for electrical conductivity measurements. Some researchers have used a commercial electrical conductivity meter (YSI model 30, YSI Incorporated, Yellow Springs, OH) to determine the conductivity of various food groups. In addition to temperature, the electrical conductivity of foods is strongly affected by ionic content, moisture mobility, and physical structure, as well as the heating process. Some researchers have studied the changes in electrical conductivity of foods during Ohmic and conventional heating . They concluded that the behavior of electrical conductivity during both treatments was different. As a result, a device was developed to determine the electrical conductivity of foods under Ohmic or conventional heating conditions. The device consists of a cylindrical sample chamber made of steel tube that contains a Teflon sleeve inside with a thermocouple opening at the center and rhodium plated stainless steel electrodes at both ends. The tube is fitted with a metallic jacket with a thermocouple opening and an inlet and outlet for circulating heat exchange fluids. A T-type copper-constantan, Teflon® coated thermocouple, with a compression fitting, is used to measure the temperature at the geometric center of the sample. Voltage and current transducers are used to measure the voltage across and the current

through the samples. Experimental data on electrical conductivity measured for several food groups have been expressed in mathematical relationships. These models are useful in estimating the electrical conductivity of food materials. Some are presented in the following. Researchers have reported that electrical conductivity is a linear function for temperature and presented the following model to predict the conductivity of solid foods:

$$\sigma_T = \sigma_{P25} [\, 1 + k\,(T - 25)] \qquad (2.35)$$

where σ_T = electrical conductivity (S/m) at any temperature T (°C), σ_{p25} = electrical conductivity of particulate at 25°C, and K = temperature compensation constant.

In this section to observe the electrical conductivity of various pure liquids, ionic solids, metals and aqueous solutions using a conductivity probe and LED conductivity indicator.

- **Electrical conductivity of molten ɛcompounds***:*

  Ionic compounds, in the solid state, are composed of ions that are not free to move. The ions become mobile after the compound is heated to its melting temperature, becomes fluid, and the ions are freed from their positions in their crystalline lattice. The large number of mobile ions then causes the molten compounds to become good electrical conductors. Covalent compounds do not conduct electricity even when molten because the resultant mobile particles are neutral molecules. Their movement cannot be used to carry an electric charge [26].

- **Electrical conductivity of metallic solids**:

Metals conduct electricity in the solid state because the valence electrons of the atoms generate a mobile “sea” of electrons.

- **Electrical conductivity of compounds in aqueous solutions**:

Water is a good solvent for many covalent and ionic compounds. Substances that dissolve in water to form electrically conducting solutions are **electrolytes**. Substances that dissolve to form no conducting solutions are known as ***nonelectrolytes***. All soluble ionic compounds are electrolytes. Water molecules are able to pull the positively and the negatively charged ions away from each other in the solid state, and carry them along to be distributed throughout the solution.

$$NaCl(S) \xrightarrow{H_2O} Na^+ + Cl^-(aq) \qquad (2.36)$$

Most covalent compounds are nonelectrolytes. When dissolved, molecules of covalent compounds are separated from each other by water molecules. The separated molecules are not charged species and will not conduct electricity. However, some covalent compounds actually react with water to form ions. The process of forming ions in this manner is known as ionization.

$$HCl(g) + H_2O\ (1) \ \rightarrow \ H_3O^+(aq) + Cl^-(aq) \qquad (2.37)$$

If all dissolved molecules react to form ions, the solution becomes strongly conducting and the solutes are referred to as strong electrolytes. If only a fraction of the dissolved molecules ionizes the solution becomes weakly conducting and the compound is known as a weak electrolyte.

$$HC_2H_3O(aq) + H_2O(1) \quad H_3O^+(aq) + C_2H_3O_2^-(aq) \qquad (2.38)$$

2.12 Previous studies:

A thin film of ($Ba_xFe_{1-x}TiO_4$) (x=1, 0.1, 0.2, 0.3, 0.5, 0.6, 0.7,08, 0.9 and 0) were prepared by the sol- gel method. The optical properties of the samples were studied using x-ray diffraction (XRD), and UV-VIS spectroscopy. The Nano crystal structure were determined using X-ray diffraction (XRD) technique. The

results show that for all samples the Nano size decreases upon decreasing iron concentration. The UV-visible spectra showed that the energy gap decreases as iron concentration decrease. The conductivity increases when Fe concentration increases for shorter wavelengths and decreases for long wavelength [33]. The conductivity increases upon increasing Fe concentration and the Nano size as well. Different papers agree with this work [34, 35, 36].

Another work was done to prepare ($Ba_xFe_{1-x}TiO_4$) (x=1, 0.1, 0.2, 0.3, 0.5, 0.6, 0.7,08, 0.9 and 0) thin film. The Nano structures of the samples were studied by using x-ray diffraction (XRD), and the optical properties were found using UV-VIS spectrometer. The X-ray diffraction (XRD) analyses show that the Nano size decreases upon decreasing iron concentration. UV-visible absorption spectra show that decreasing iron concentration increases absorption coefficient. Decreasing Nano size, increases absorption coefficient [37].
Increasing Fe concentration also increases crystal size and crystal spacing. This study conforms with other studies [38, 39, 40].

Thin films of $(ZnO)_x$ $(Al_2O_3)_{1-x}$ deposited on glass substrates by were prepared by changing ZnO concentration from 0 to 1 in steps of 0.1. To
determine the absorption coefficient and the energy gap UV spectrum was used. The Nano crystal size was determined using the x-ray diffraction (XRD) technique. The results show that the absorption
coefficient decreases upon decreasing the Nano crystal size and the energy gap decreases when the ZnO concentration decreases from 0.9 to 0.3 [41]. The absorption coefficient of $(ZnO)_x(Al_2O_3)$1-x thin film decreases as the Nano crystal size decreases. The energy gap decreases when ZnO concentration decreases up to 0.3. This work is agrees with many researches [42, 43, 44].
$CH_3NH_3PbI_3$ planar-structure perovskite solar cells were fabricated with the configuration FTO/ZnO/ $CH_3NH_3PbI_3$/Au. To study crystal Nano structure, Nano size and optical properties XRD, SEM, UV-visible and I–V techniques,

were used for the performance of the cells. The best cell performance was achieved for the perovskite solar cell with a ZnO film coated by the spin method. The average efficiency was 7% without using any hole transport materials and 10.25% using spiro-OMeTAD as a hole transport material. The average efficiencies of the cells coated by the spraying and SILAR methods using spiro-OMeTAD, were found to be 8.64% and 7.7% respectively. This study demonstrates the versatility of the spray and SILAR coating methods and their potential for fabricating low-cost, perovskite solar cells [45].

Dye sensitized solar cells were fabricated from: Ecrchrom Black T, DDTTC, Rhodamine B, and Coumarin 500, with Al and TTO electrodes. The energy gab was found using UV technique. The energy gap for: Ecrchrom Black T, DDTTC, Rohadamin B, and Coumarin 500; were found to be 2.16 eV ,2.20 eV ,3.27 eV and 3,60 respectively. The efficiency of Ecrchrom Black T, DDTTC, Rohadamin B, Coumarin 500 were found to be 1.66,1.62, 1.49 and 1.31 respectively. Thus, the efficiency increases when the energy gab decreases [46,47,48.49]. A lot of conform with this work [50, 51,52].

The oxides Tio_2, CuO, ZnO, and MgO, were used to dope carbon Nano tube at different annealing temperatures.450 ,500 ,550, and 600 C0. The conductivity and dielectric constants were determined at different annealing temperatures. It was found that the conductivity and dielectrics constants decrease upon increasing the temperature except for MgO where they increase [53].

Thin films of ($Ba_xFe_{1-x}TiO_4$) (x=1, 0.1, 0.2, 0.3, 0.5, 0.6, 0.7,08, 0.9 and 0) were fabricated. The effect of changing Fe concentration on the structural and optical properties of the samples were studied using x-ray diffraction (XRD), and UV-VIS spectroscopy respectively. The X-ray diffraction (XRD) technique indicates the Nano size decreases upon decreasing iron concentration. The UV-visible spectra showed that the energy gap decreases from (2.074) eV to (2.046) eV as iron concentration decrease. The conductivity increases when Fe concentration

increases for shorter wavelengths and decreases for longer wavelengths. The energy gap decreases as the Nano size decreases. The conductivity increases upon increasing Fe concentration and the Nano size as well. This work was confirmed many previous studies [54, 56, 57].

3.13 Summary and critique:

The UV spectrometer and other visible light spectrometers can be used to study electrical magnetic [58, 59, 60, 61] and optical properties of matters [62, 63, 64, 65]. Nano science can be used to control these properties [66, 67, 68] to fabricate highly efficient, low-cost Nano solar cells [69, 70, 71].

Chapter Three

Material and Method

3.1 Introduction

This chapter consist of all material were used to preparation the samples of $Al_{2x}Fe_{3(1-x)}O_4$ and $Cu_xFe_{1-x}O_2$ with molar concentrations x= 0.1,0.3,0.5 ,0.7 and 0.9 , in addition to the instruments to analysis the samples to determine the optical properties , structure and frequency bonding by Using U-V spectrometer , (FTIR and XRD) and respectively.

3.2 preparations of samples

In this study ten samples of $Al_{2x}Fe_{3\ (1-x)}\ O_4$ and $Cu_xFe_{\ (1-x)}O_2$ were prepared by sol gel method. Firstly the metallic oxide of Al_2O_3CuO and FeO were prepared by dissolving aluminum Nitrate $Al(NO_3)\ 39H_2O$,copper nitrate (non hydrate) $Cu(NO_3)\ 26H_2O$ and Iron nitrate (non hydrate) Fe (NO3) 39H2O in distilled water in acidic medium in magnetic stirrer at 80 C for 60 minutes. The iron solution is then mixed with Aluminum and Copper for different concentrations (5 concentrations for each mixture) following the formula $A_{l2x}Fe_3\ (1\text{-}x)O_2$ and $Cu_xFe(1\text{-}x)O_2$. After gel formation the samples were exposed to the atmosphere for 24 hours. To make the samples in a powder form they are deried in oven for 2 hours. They are then characterized using x ray diffraction technique (XRD), to get structure parameters. The UV-visible spectrometer was used to study optical and electrical properties. The (FTIR) was utilized to study atomic vibrational modes.

3.2.1 Aluminum Oxide

Aluminum oxide is a chemical compound of aluminum and oxygen with the chemical formula Al_2O_3. It is the most commonly occurring

several aluminum oxides, and specifically identified as aluminum (III) oxide. It is commonly called alumina and may also be called AL oxide, or alundum depending on particular forms or applications. It occurs naturally in its crystalline polymorphic phase α-Al_2O_3 as the mineral corundum, varieties of which form the precious gemstones ruby and sapphire. Al_2O_3 is significant in its use to produce aluminum metal, as an abrasive owing to its hardness, and as a refractory material owing to its high melting point The samples of Al_2O_3 were prepped from Aluminum nitrate (nonahydrate) extra pure $Al(NO_3)_3.9H_2O$

3.2.2 Ethanol

Ethanol is a natural byproduct of plant fermentation and also can be produced through the hydration of ethylene. Ethanol, also called alcohol with chemical formula C_2H_6O, ethyl alcohol and grain alcohol, is a clear, colorless liquid and the principal ingredient in alcoholic beverages like beer, wine or brandy. Because it can readily dissolve in water and other organic compounds, ethanol also is an ingredient in a range of products, from personal care and beauty products to paints and varnishes to fuel.

3.2.3 Distillation Water

Distilled water is water that has been boiled into vapor and condensed back into liquid in a separate container. Impurities in the original water that do not boil below or near the boiling point of water remain in the original container. Thus, distilled water is a type of purified water (H_2O).

3.3 Characterization Techniques

The Materials Characterization Lab has a wide variety of characterization techniques in the areas of X-ray diffractometer, FTIR (Fourier Transform Infrared Spectrophotometer), and min 1240 UV- Spectroscopy techniques which help to increase the different degrees of understanding why different materials show different properties and behaviors. To investigate the optical properties of

Gum Arabic (Hashaba) doping by aluminum oxide made by two methods, some precise techniques have been used in our stud. The following characterizations have been potentially performed for the analytical of the synthesized samples.

3.3.1 Fourier Transport Infrared Spectroscopy (FTIR)

A technique used to obtain an infrared spectrum of absorption or emission of a solid, liquid or gas. An FTIR spectrometer simultaneously collects high-resolution spectral data over a wide spectral range. This confers a significant advantage over a dispersive spectrometer, which measures intensity over a narrow range of wavelengths at a time. The goal of absorption spectroscopy techniques (FTIR, ultraviolet-visible ("UV-Vis") spectroscopy, etc.) is to measure how much light a sample absorbs at each wavelength. The most straightforward way to do this, the "dispersive spectroscopy" technique, is to shine a monochromatic light beam at a sample, measure how much of the light is absorbed, and repeat for each different wavelength. (This is how some UV–vis spectrometers work**.** Fourier transport infrared (FTIR) spectra of samples were detected by (Mattson, Model 960m0016) spectra with transmission from 4000 to 400cm^{-1}, by using KBr pellets seen. Show in fig (3.1).

Figure (3.1): FTIR (Mattson, model 960m0016) spectroscopy.

3.3.2 Ultraviolet -visible spectroscopy (UV-Vis)

Absorption of light in the UV/Visible part of the spectrum (210 – 900 nm). The transitions that result in the absorption of electromagnetic radiation in this region of the spectrum are transitions between electronic energy levels. Generally, the most probable transition is from highest occupied molecular orbital (HOMO) to lowest occupied molecular orbital (LUMO). Light in the UV-VIS part of the spectrum is used to promote electrons from the ground state to various excited states. The particular frequencies at which light is absorbed are affected by the structure and environment of the chromosphere (light absorbing species). Excited electrons can return to the ground state by vibrational transitions through smaller energy increments. Absorbed energy appears ultimately as heat in solution. The absorption spectra of prepared nanoparticles were measured using shimadzu spectrophotometer (UV mini-1240) in 190-800nm range see Figure (3.2)

Fig (3.2): UV mini 1240 spectrometer shimadzu

3.3.3 X-ray Powder Diffraction (XRD):

X-ray powder diffraction (XRD) is a rapid analytical technique primarily used for phase identification of a crystalline material and can provide information on unit cell dimensions. The analyzed material is finely ground, homogenized, and average bulk composition is determined. (XRD) is a non-destructive technique for analyzing the structure of materials, primarily at the atomic or molecular level. It works best for materials that are crystalline or partially crystalline (i.e., that have periodic structural order) but is also used to study non-crystalline materials. XRD relies on the fact that X-rays are a form of light, with wavelengths on the order of nanometers. When X-rays scatter from a substance with structure at that length scale, interference can take place, resulting in a pattern of higher and lower intensities. This is qualitatively similar to the colorful patterns produced by soap bubbles, in which different colors are viewed in different directions.XRD produces a diffraction pattern, which does not superficially resemble the underlying structure, and provides information about the internal structure on length scales from 0.1 to 100 nm. A beam of X-rays is directed towards a sample, and the scattered intensity is measured as a function of outgoing direction. By convention, the angle between the incoming and outgoing beam directions is called 2θ. For the simplest possible sample, consisting of sheets of charge separated by a distance *d*, constructive interference (greater scattered intensity) is observed when Bragg's Law is satisfied: $n\lambda = 2d \sin\theta$ Here *n* is an integer (1, 2, 3 ...) λ is the wavelength of the x-ray beam, and θ is half the scattering angle 2 θ shown above. Real materials are more complicated, of course, but the general result holds that there is a relationship between interparticle distances within the sample and the angles at which the scattered intensity is the highest, with larger distances *d* corresponding to smaller scattering angles 2θ.the data collected by using X-Ray diffract meter: XRD (wavelength 1.54 A°) in the figure below

Fig (3.3) X-Ray diffract meter: XRD (wavelength 1.54 A°),

Chapter Four

Results and Discussion

4.1 Introduction

In this chapter samples of ($Al_{2x}\ Fe_{3(1-x)}\ O_4$ and $Cu_xFe_{1-x}\ O_2$) (0.1 ,0.3 ,0.5 ,0.7 and 0.9) are analyzed. The data of X-ray diffraction (XRD) have been analyzed by using Rietveld method to study their crystal and nanostructure, their lattice parameters, the positions of atoms within the cell, the UV-visible is used to evaluate the band gap and optical properties beside electrical and magnetic properties from optical method.

4.2 X-ray diffraction (XRD) Results of ($Al_{2x}\ Fe_{3(1-x)}\ O_4$) samples

The diffraction peaks of x-ray were displayed the following figure

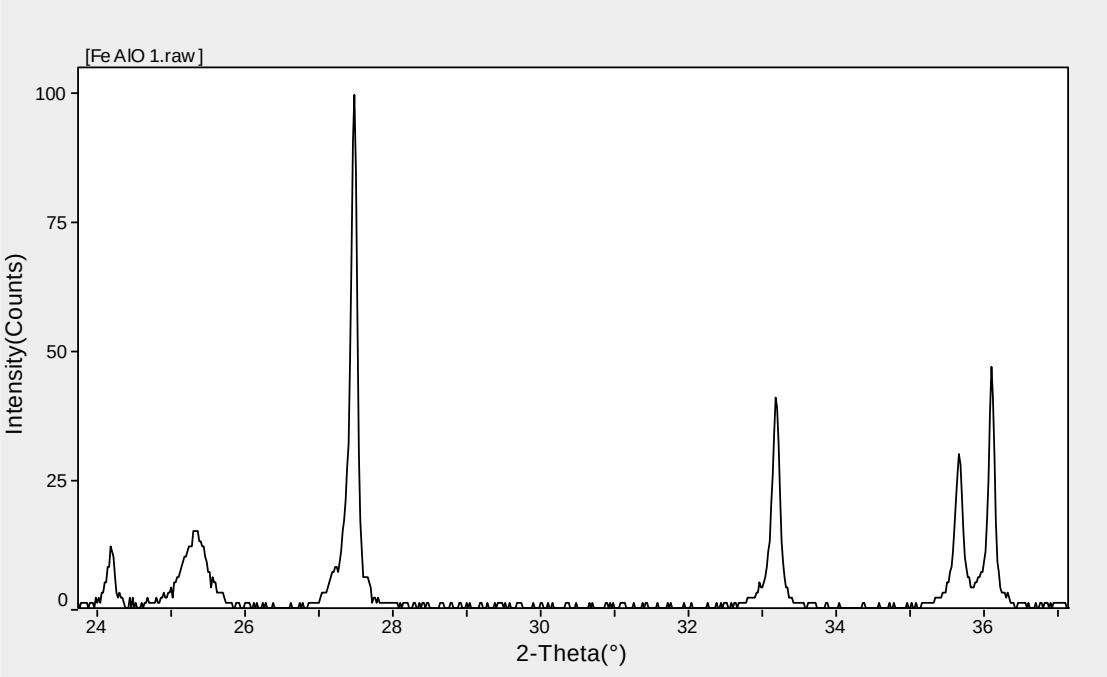

Fig (4.1) XRD spectrum of $Al_{0.2}Fe_{0.9}O_4$ sample

Table (4.1) Lattice Constants from Peak Locations and Miller Indices [Tetragonal – primitive] of $Al_{0.2}Fe_{0.9}O_4$ sample

2 theta	d(A^O)	h k l	X_s (nm)
25.339	3.5143	1 1 2	30.6
27.479	3.2416	1 1 0	100
33.182	2.6957	1 2 1	74.4
35.661	2.5141	1 0 1	88.9
36.101	2.4844	1 1 1	100

d = distance between adjacent crystal planes

X_S = crystal nano size

C. form = Tetragonal – primitive

G. space = P42/m n m (136)

a = b = 4.568 c = 2.964

$\alpha = \beta = \gamma = 90^O$

Cell volume = 61.8 density = 7.3065 $mg.cm^{-3}$

Average lattice constants = 5.8928

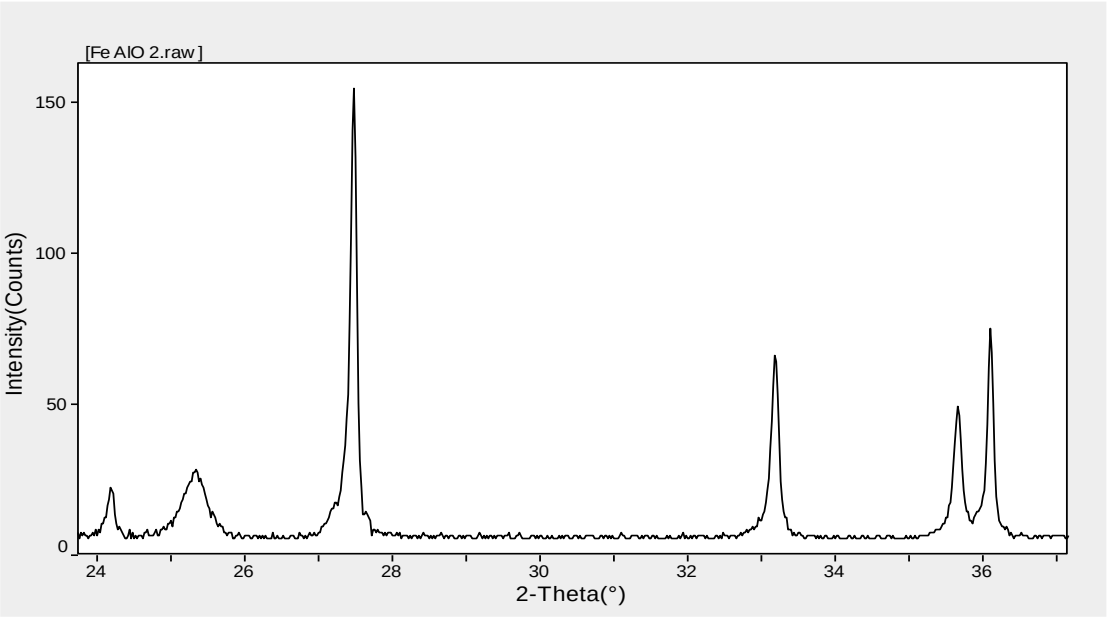

Fig (4.2) XRD spectrum of $Al_{0.6}Fe_{0.7}O_4$ sample

Table (4.2) Lattice Constants from Peak Locations and Miller Indices [Tetragonal – primitive] of $Al_{0.6}Fe_{0.7}O_4$ sample

2 theta	d(A^O)	h k l	X_s (nm)
25.339	3.2437	1 1 2	100
27.479	2.6978	1 1 0	100
33.182	2.5158	1 2 1	100
35.661	2.4860	1 0 1	100

d = distance between adjacent crystal planes

X_S = crystal Nano size

C. form = Tetragonal – primitive

G. space = P42/m n m (136)

a = b = 4.568 c = 2.964

$\alpha = \beta = \gamma = 90^O$

Cell volume = $(61.8A^O)^2$ density = 7.3065 $mg.cm^{-3}$

Average lattice constants = 5.3928

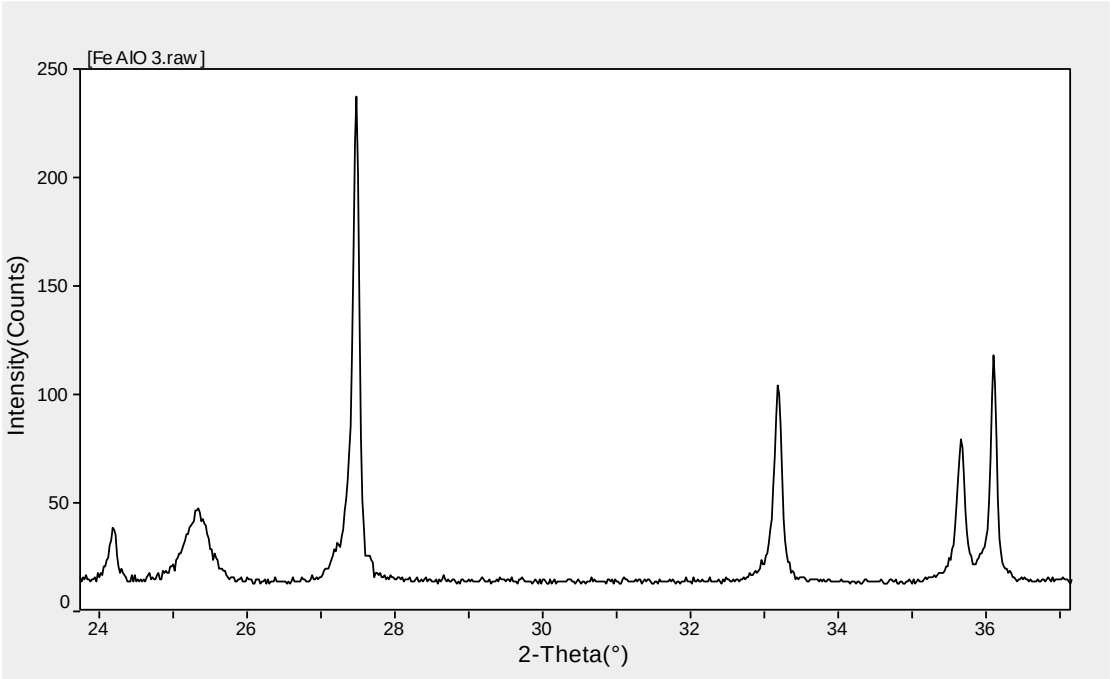

Fig (4.3) XRD spectrum of $Al_{1.0}Fe_{0.5}O_4$ sample

Table (4.3) Lattice Constants from Peak Locations and Miller Indices [Tetragonal – primitive] of $Al_{1.0}Fe_{0.5}O_4$ sample

2 theta	d(A^O)	h k l	X_s (nm)
25.339	3.5121	1 1 2	25.5
27.479	3.2432	1 1 0	100
33.182	2.6976	1 2 1	81.2
35.661	2.5156	1 0 1	55.3
36.101	2.4859	1 1 1	86.7

d = distance between adjacent crystal planes

X_S = crystal nano size

C. form = Tetragonal – primitive

G. space = P42/m n m (136)

a = b = 4.568 c = 2.964

$\alpha = \beta = \gamma = 90^O$

Cell volume = $(61.8\ A^O)^2$ density = 7.3065 $mg.cm^{-3}$

Average lattice constants = 5.0581

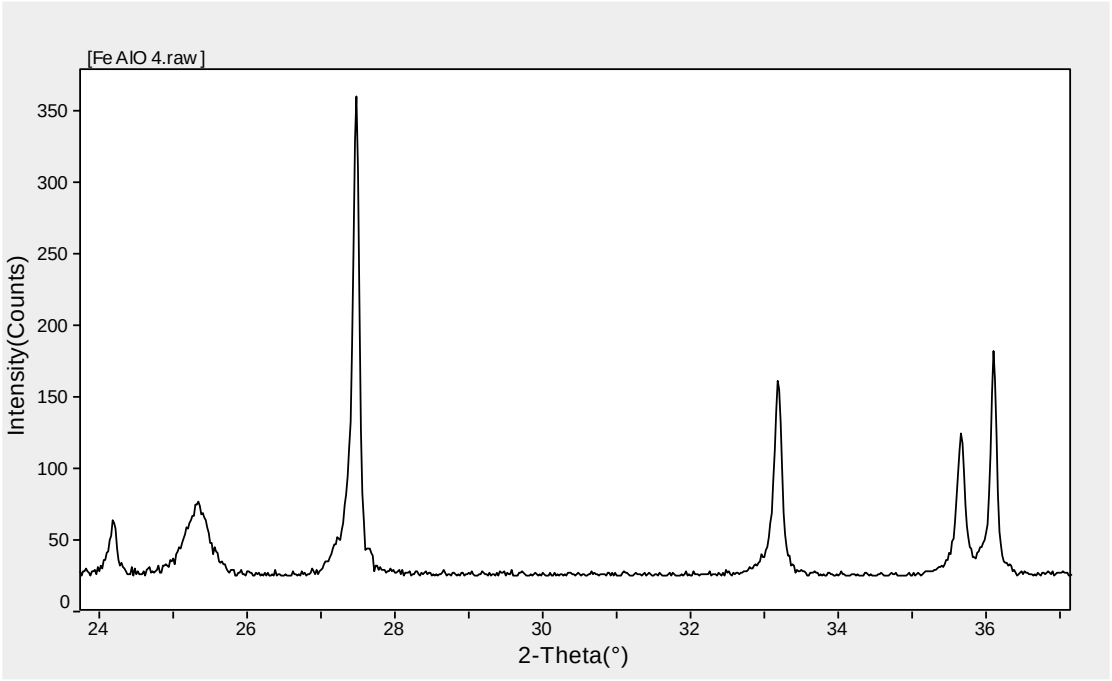

Fig (4.4) XRD spectrum of $Al_{1.4}Fe_{0.3}O_4$ sample

Table (4.4) Lattice Constants from Peak Locations and Miller Indices [Tetragonal – primitive] of $Al_1.Fe4_{0.3}O_4$ sample

2 theta	d(A^O)	h k l	X_s (nm)
25.339	3.5121	1 1 2	25.4
27.479	3.2432	1 1 0	100
33.182	2.6976	1 2 1	85.5
35.661	2.5156	1 0 1	58.5
36.101	2.4859	1 1 1	100

d = distance between adjacent crystal planes

X_S = crystal nano size

C. form = Tetragonal – primitive

G. space = P42/m n m (136)

A = b = 4.568 c = 2.964

$\alpha = \beta = \gamma = 90^O$

Cell volume = $(61.8A^O)^2$ density = 7.3065 $mg.cm^{-3}$

Average lattice constants = 5.0573

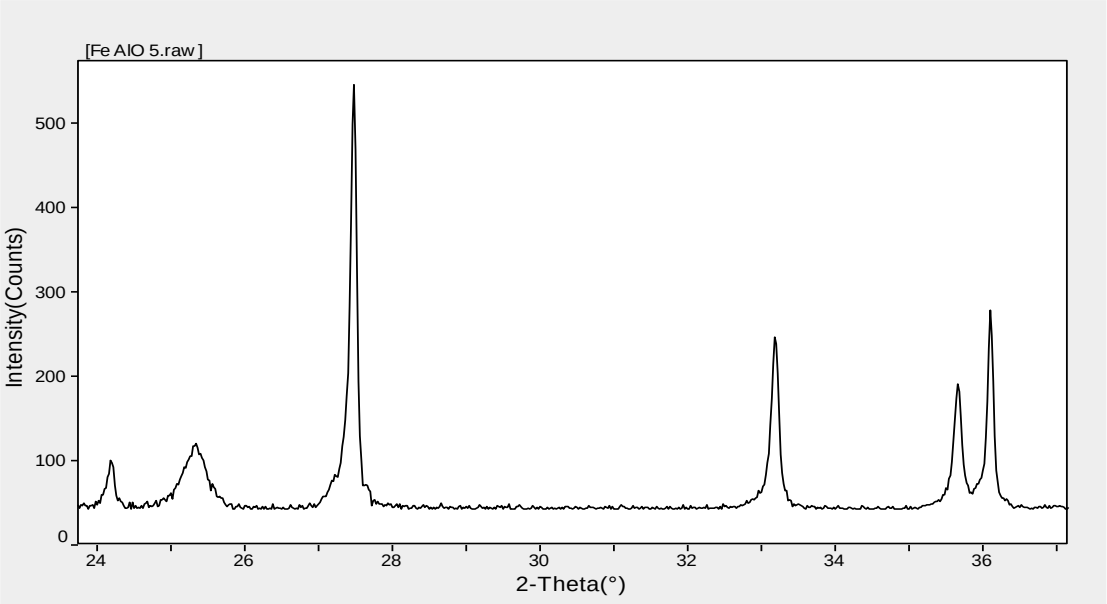

Fig (4.5) XRD spectrum of $Al_{1.8}Fe_{0.1}O_4$ sample

Table (4.5) Lattice Constants from Peak Locations and Miller Indices [Tetragonal – primitive] of $Al_{1.8}Fe_{0.1}O_4$ sample

2 theta	d(A^O)	h k l	X_s (nm)
25.339	3.5121		24.9
27.479	3.2432	1 1 0	100
33.182	2.6977	1 2 1	82
35.661	2.5156	1 0 1	55.4
36.101	2.4859	1 1 1	100

d = distance between adjacent crystal planes

X_S = crystal nano size

C. form = Tetragonal – primitive

G. space = P42/ m n m (136)

a = b = 4.568 c = 2.964

a= b= g = 90 ^{O}

Cell volume = $(61.8A^O)^2$ density = 7.3065 $mg.cm^{-3}$

Average lattice constants = 5.0569

4.3 X-ray diffraction (XRD) Results of ($Cu_x Fe_{(1-x)} O_4$) samples

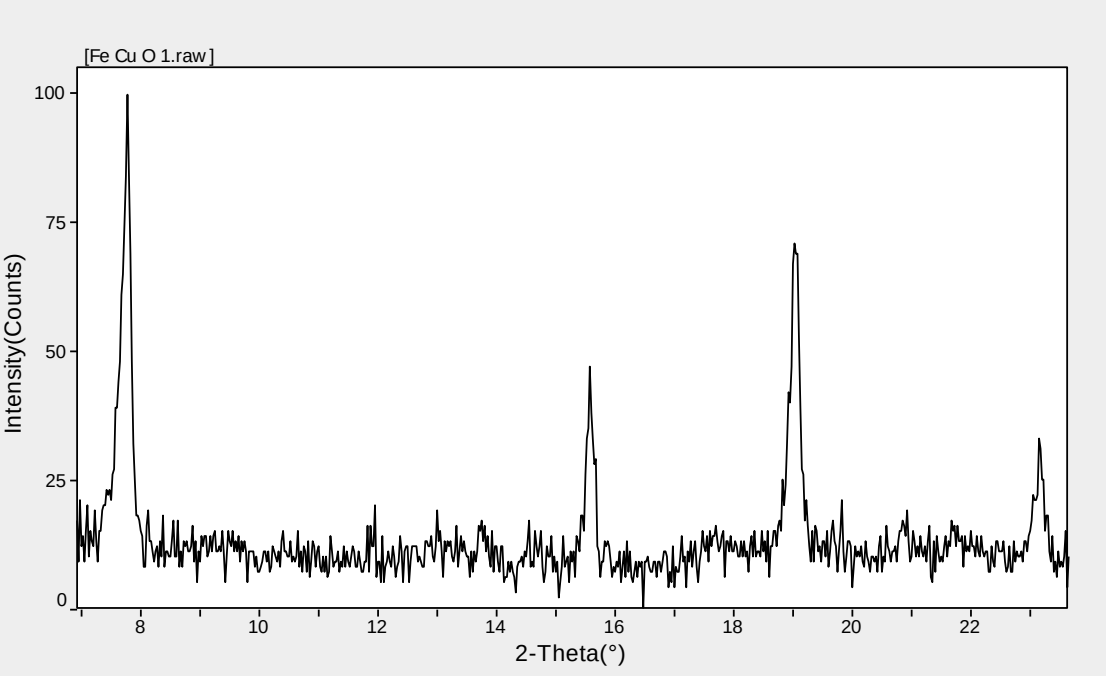

Fig (4.6) XRD spectrum of $Cu_{0.1}Fe_{0.9}O_4$ sample

Table (4.6) Lattice Constants from Peak Locations and Miller Indices [Hexagonal – primitive] of $Cu_{0.1}Fe_{0.9}O_4$ sample

2 theta	d(A^O)	h k l	X_s (nm)
7.772	11.3654	0 0 2	100
15.571	5.682	0 1 0	100
19.027	4.6605	1 3 1	98.3

C. form = hexagonal – primitive

G. space = R - 3m (166)

A = b = 3.47 c = 34.5

$\alpha = \beta = 90^O$ $\gamma = 120^O$

Cell volume = $(359.8\ A^O)^2$ density = 3.9473 $mg.cm^{-3}$

Average lattice constants = 19.5768

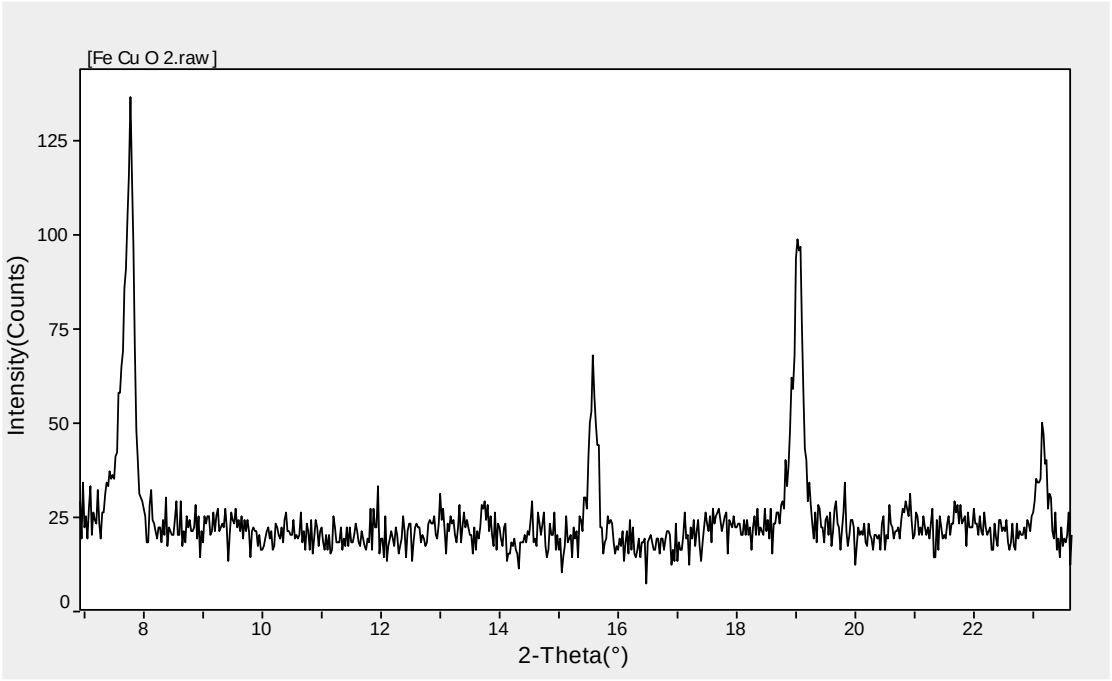

Fig (4.7) XRD spectrum of $Cu_{0.3}Fe_{0.7}O_4$ sample

Table (4.7) Lattice Constants from Peak Locations and Miller Indices [Hexagonal – primitive] of $Cu_{0.3}Fe_{0.7}O_4$ sample

2 theta	d(A^O)	h k l	X_s (nm)
7.772	11.3627	0 0 2	54.8
15.571	5.6846	0 1 0	67.1
19.027	4.6599	1 3 1	46.9

C. form = hexagonal – primitive

G. space = R - 3m (166)

a = b = 3.47 c = 34.5

$\alpha = \beta = 90^O$ $\gamma = 120^O$

Cell volume = $(359.8A^O)^2$ density = 3.9473 $mg.cm^{-3}$

Average lattice constants = 19.5781

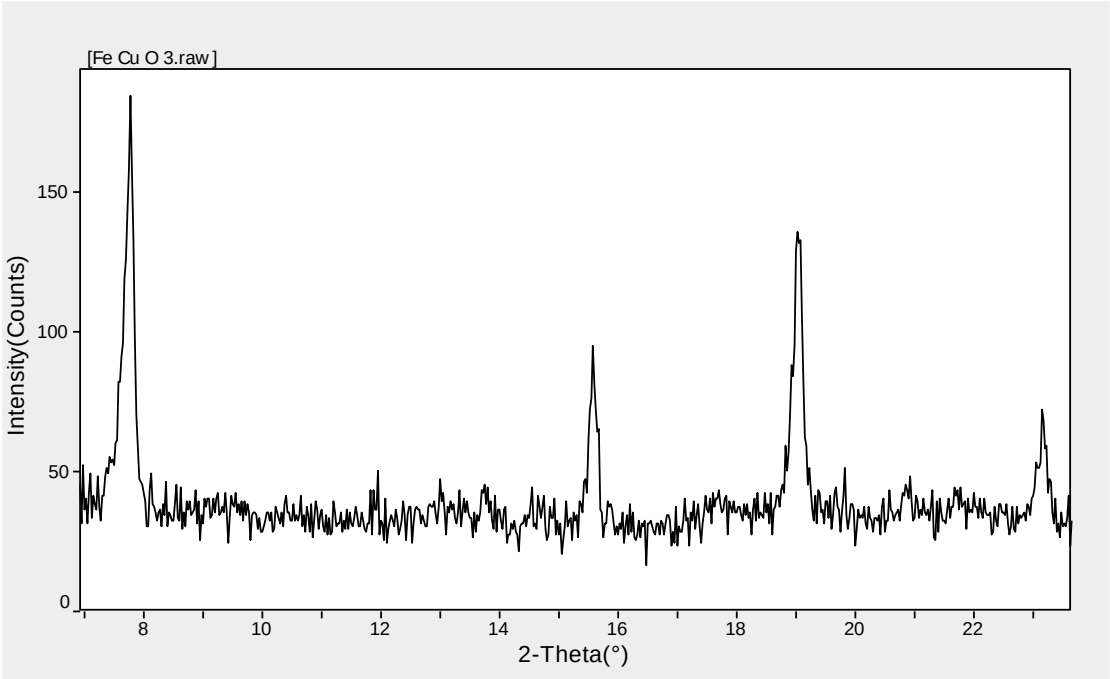

Fig (4.8) XRD spectrum of $Cu_{0.5}Fe_{0.5}O_4$ sample

Table (4.8) Lattice Constants from Peak Locations and Miller Indices [Hexagonal – primitive] of $Cu_{0.5}Fe_{0.5}O_4$ sample

2 theta	d(A^O)	h k l	X_s (nm)
7.772	11.3628	0 0 2	54.9
15.571	5.6864	0 1 0	65.3
19.027	4.6599	1 3 1	43.2

C. form = hexagonal – primitive

G. space = R - 3m (166)

A = b = 3.47 c = 34.5

$\alpha = \beta = 90^O$ $\gamma = 120^O$

Cell volume = $(359.8A^O)^2$ density = 3.9473 $mg.cm^{-3}$

Average lattice constants = 19.5813

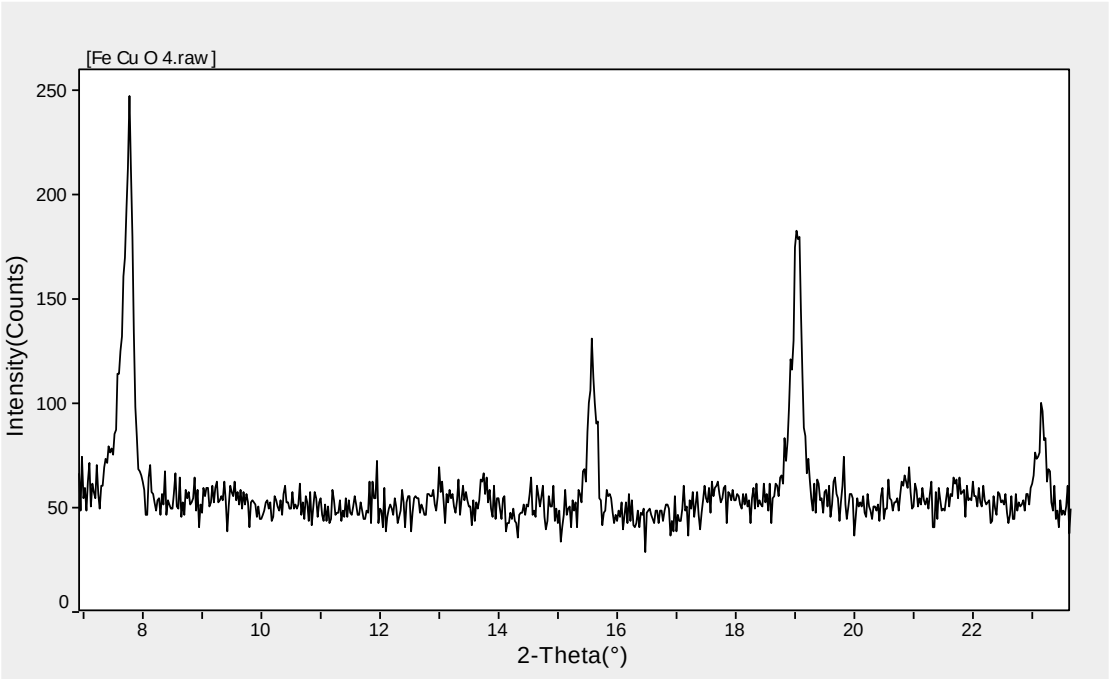

Fig (4.9) XRD spectrum of $Cu_{0.7}Fe_{0.3}O_4$ sample

Table (4.9) Lattice Constants from Peak Locations and Miller Indices [Hexagonal – primitive] of $Cu_{0.7}Fe_{0.3}O_4$ sample

2 theta	d(A^O)	h k l	X_s (nm)
7.772	11.3628	0 0 2	54.1
15.571	5.6846	0 1 0	68.1
19.027	4.6599	1 3 1	43

C. form = hexagonal – primitive

G. space = R - 3m (166)

A = b = 3.47 c = 34.5

$\alpha = \beta = 90^O$ $\gamma = 120^O$

Cell volume = $(359.8A^O)^2$ density = $3.9473 mg.cm^{-3}$

Average lattice constants = 19.5749

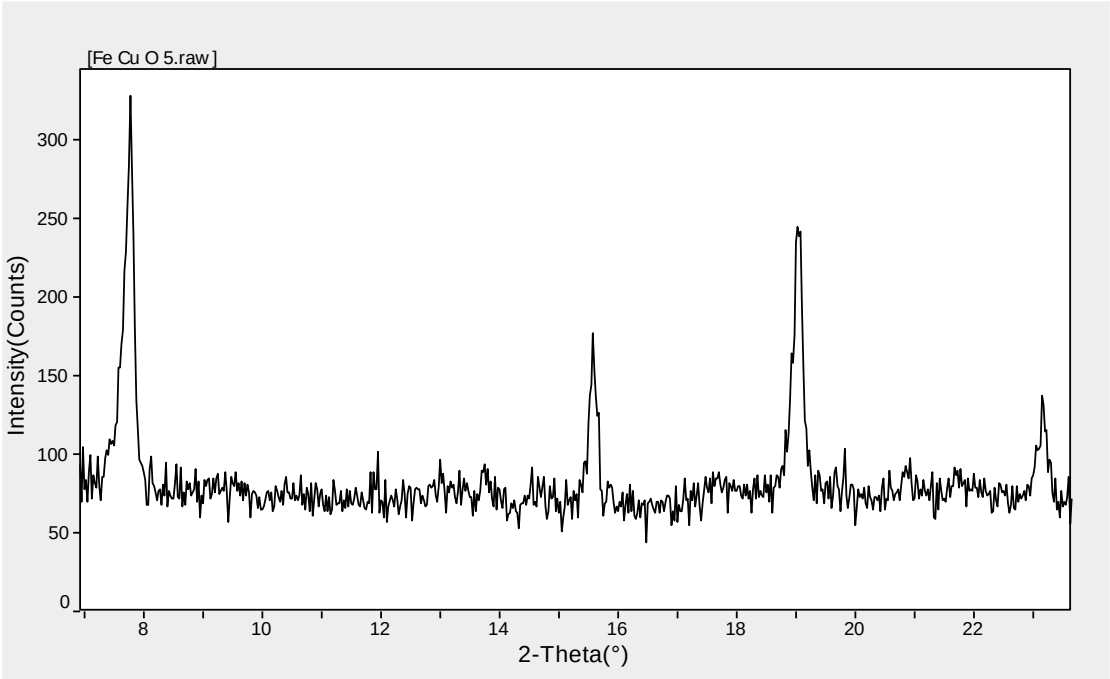

Fig (4.10) XRD spectrum of $Cu_{0.1}Fe_{0.9}O_4$ sample

Table (4.10) Lattice Constants from Peak Locations and Miller Indices [Hexagonal – primitive] of $Cu_{0.1}Fe_{0.9}O_4$ sample

2 theta	d(A^O)	h k l	X_s (nm)
7.772	11.3628	0 0 2	54.3
15.571	7.4065	0 1 0	100
19.027	5.6846	1 3 1	69.9

C. form = hexagonal – primitive

G. space = R - 3m (166)

A = b = 3.47 c = 34.5

$\alpha = \beta = 90^O$ $\gamma = 120^O$

Cell volume = $(359.8A^O)^2$ density = 3.9473 $mg.cm^{-3}$

Average lattice constants = 19.7276

4.4 Optical Results of ($Al_{2x}Fe_{3(1-x)}O_4$) sample

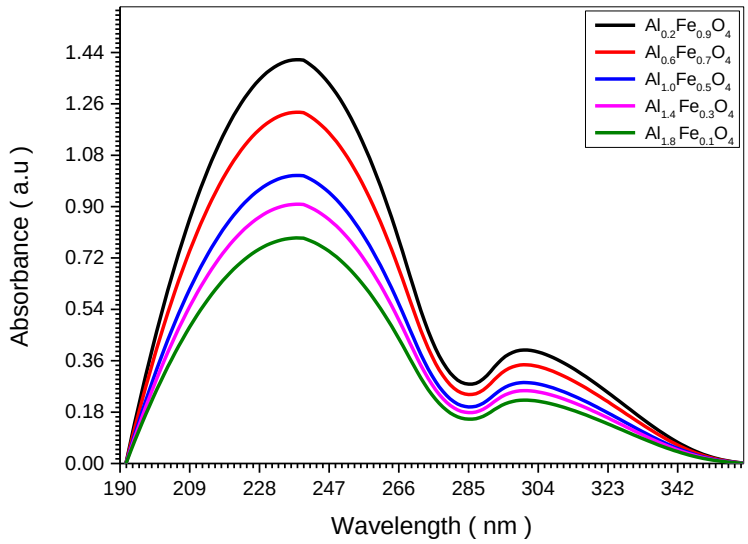

Fig(4.11) relation between absorbance and wavelengths of five ($Al_{2x}Fe_{3(1-x)}O_4$) samples (0.1 ,0.3 ,0.5 ,0.7 and 0.9) Molar concentrations

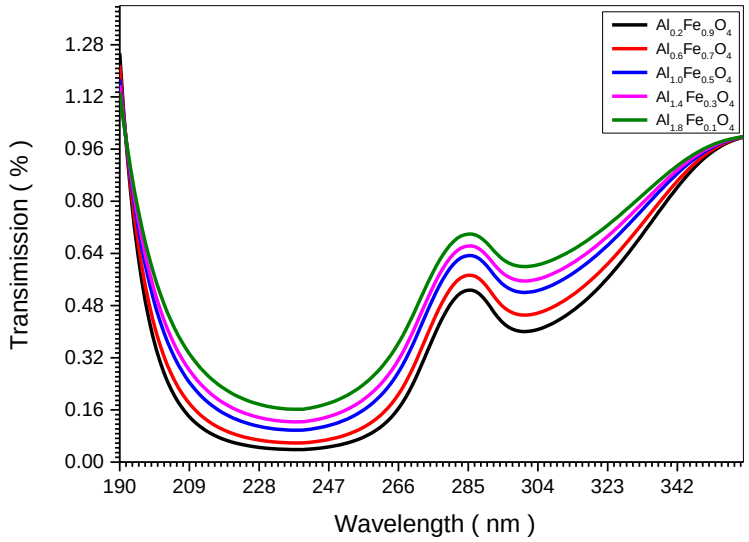

Fig(4.12) relation between Transimission and wavelengths of five ($Al_{2x}Fe_{3(1-x)}O_4$) samples (0.1 ,0.3 ,0.5 ,0.7 and 0.9) Molar concentration

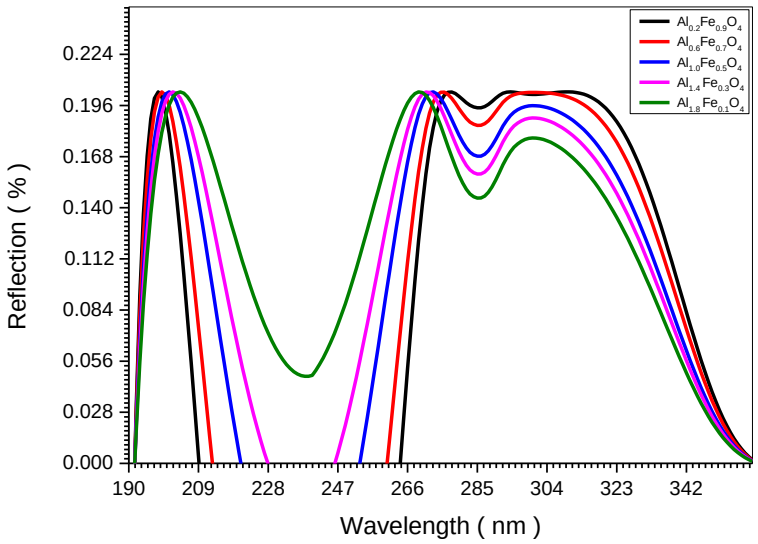

Fig(4.13) relation between Reflection and wavelengths of five ($Al_{2x}Fe_{3(1-x)}O_4$) samples (0.1 ,0.3 ,0.5 ,0.7 and 0.9) Molar concentrations

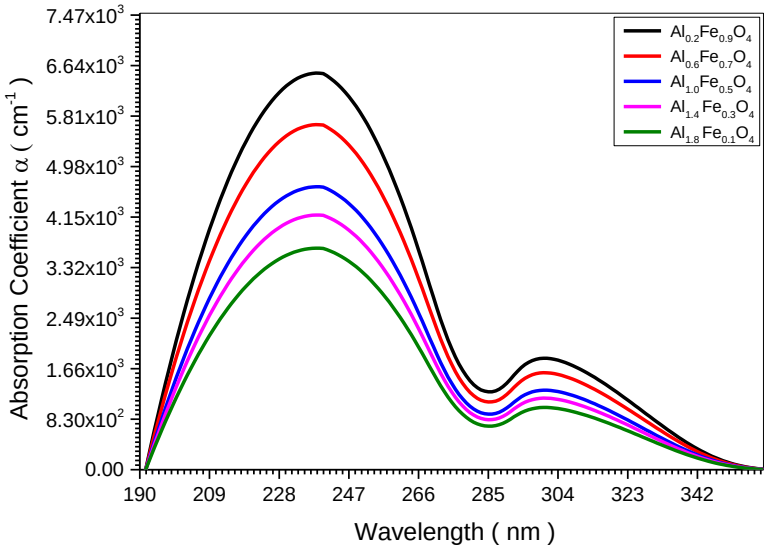

Fig(4.14) relation between absorption Coefficient and wavelengths of five ($Al_{2x}Fe_{3(1-x)}O_4$) samples (0.1 ,0.3 ,0.5 ,0.7 and 0.9) Molar concentrations

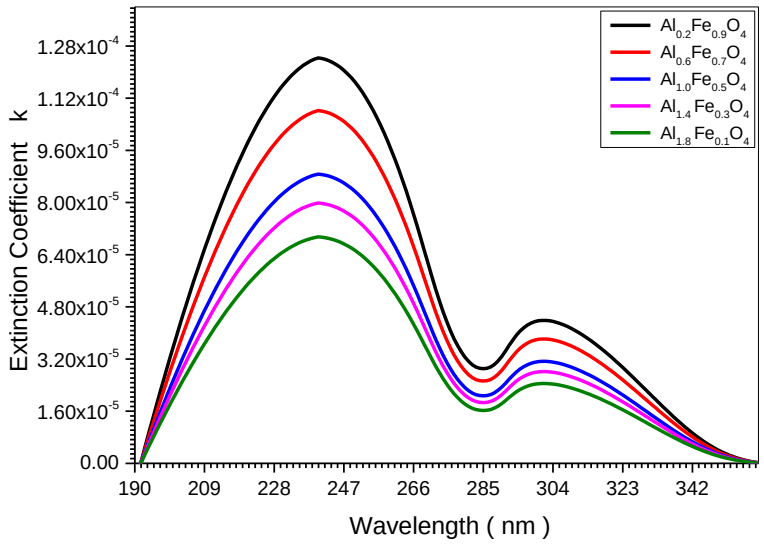

Fig(4.15) relation between exctintion coefficient and wavelengths of five (Al_{2x} $Fe_{3(1-x)}$ O_4) samples (0.1 ,0.3 ,0.5 ,0.7 and 0.9) Molar concentrations

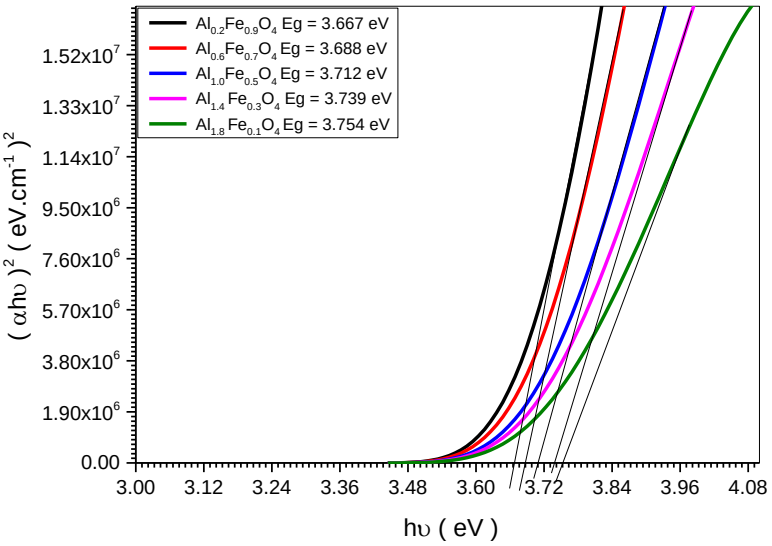

Fig(4.16) Optical energy band gap of five (Al_{2x} $Fe_{3(1-x)}$ O_4) samples (0.1 ,0.3 ,0.5 ,0.7 and 0.9) Molar concentrations

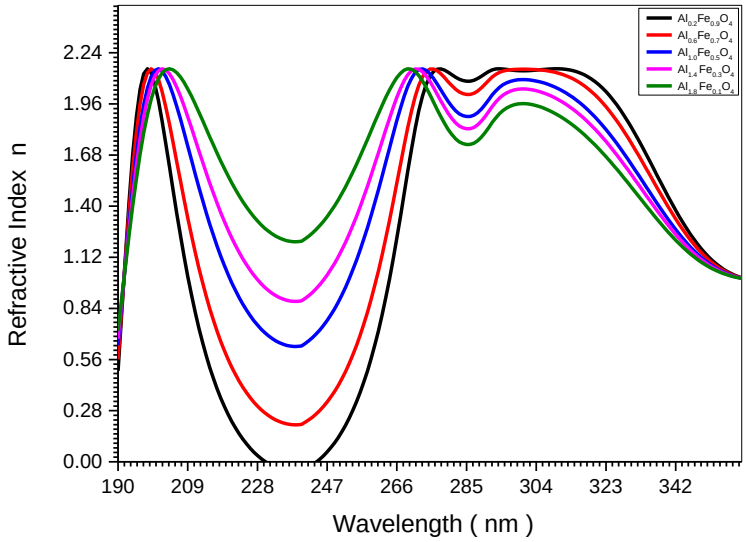

Fig(4.17) relation between refractive Index and wavelengths of five ($Al_{2x}\,Fe_{3(1-x)}\,O_4$) samples (0.1 ,0.3 ,0.5 ,0.7 and 0.9) Molar concentrations

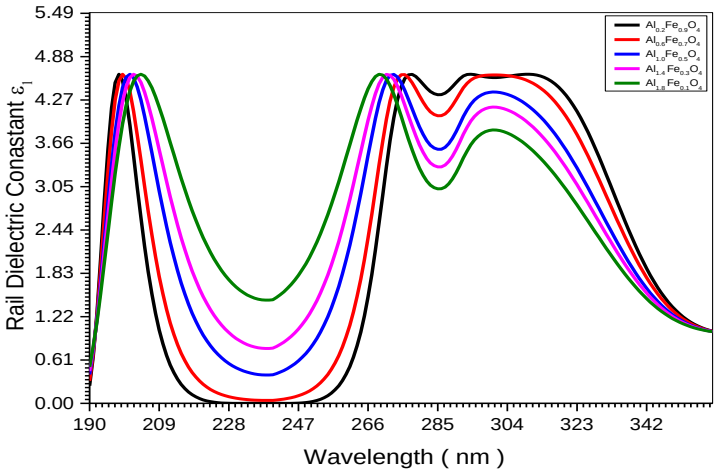

Fig(4.18) relation between rail dielectrcal constant and wavelengths of five ($Al_{2x}\,Fe_{3(1-x)}\,O_4$) samples (0.1 ,0.3 ,0.5 ,0.7 and 0.9) Molar concentrations

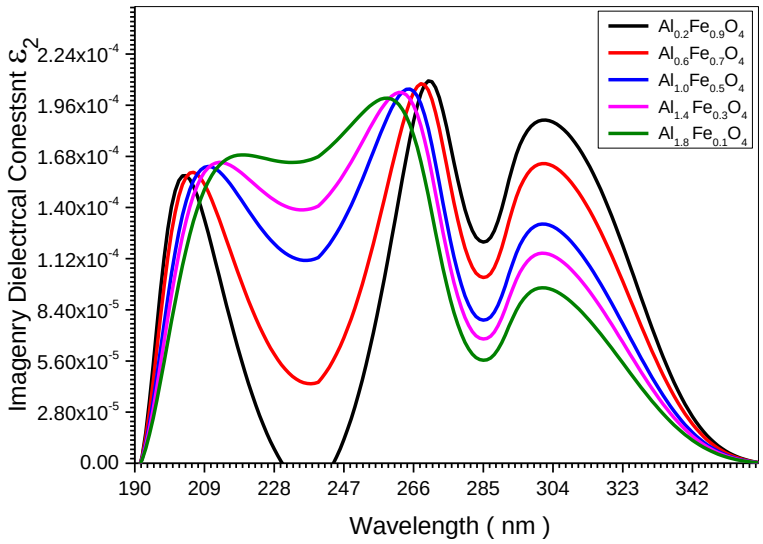

Fig(4.19) relation between Imagenary dielectracal conastant and wavelengths of five ($Al_{2x}Fe_{3(1-x)}O_4$) samples (0.1 ,0.3 ,0.5 ,0.7 and 0.9) Molar concentrations

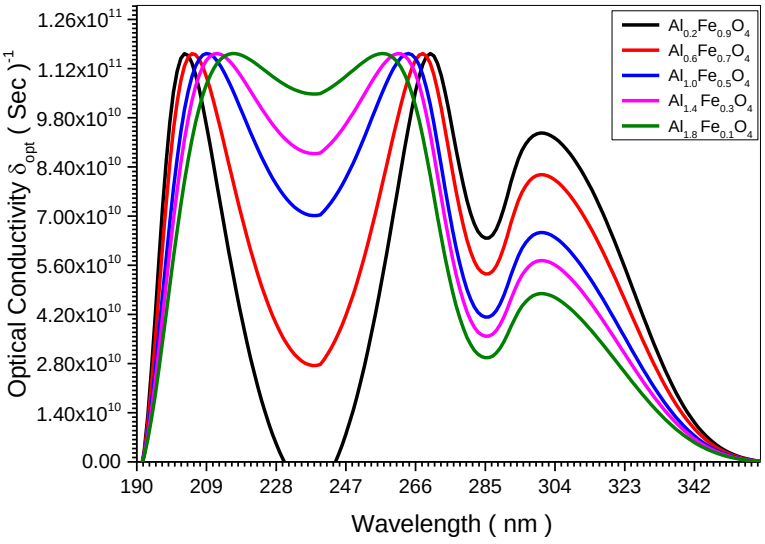

Fig(4.20) relation between Optical conductivity and wavelengths of five ($Al_{2x}Fe_{3(1-x)}O_4$) samples (0.1 ,0.3 ,0.5 ,0.7 and 0.9) Molar concentrations

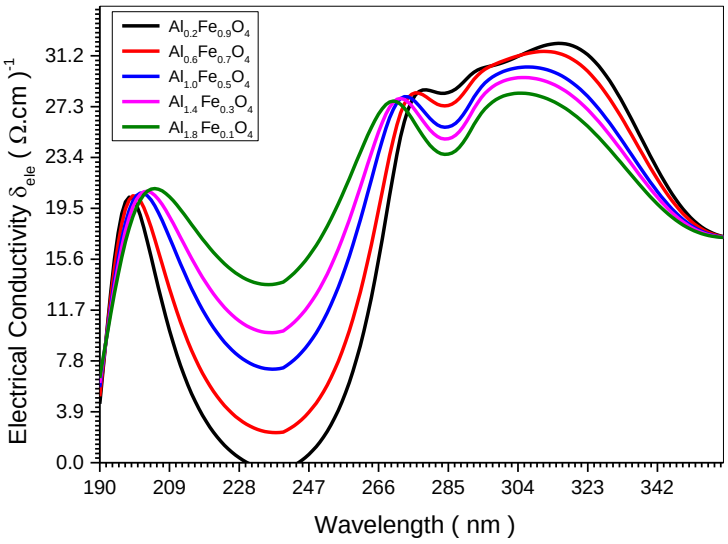

Fig(4.21) relation between electrical conductivity and wavelengths of five ($Al_{2x}Fe_{3(1-x)}O_4$) samples (0.1 ,0.3 ,0.5 ,0.7 and 0.9) Molar concentrations

4.5 Optical Results of ($Cu_xFe_{(1-x)}O_2$) sample

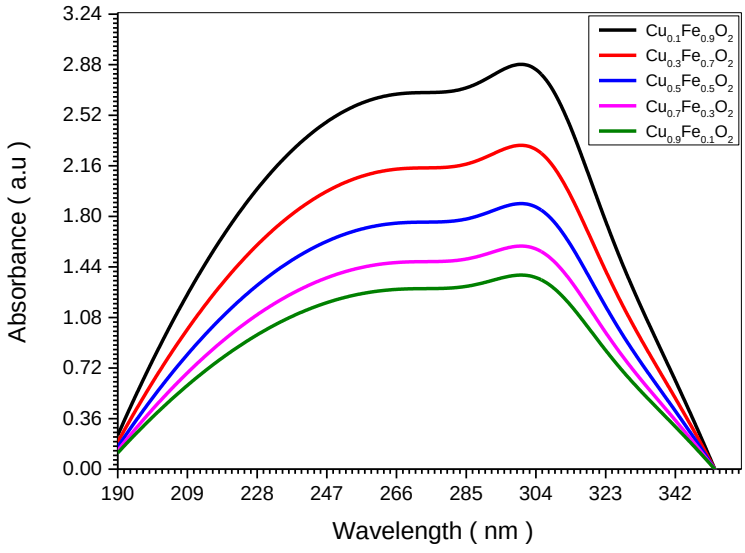

Fig(4.22) relation between absorbance and wavelengths of five ($Cu_xFe_{(1-x)}O_2$) samples (0.1 ,0.3 ,0.5 ,0.7 and 0.9) Molar concentrations

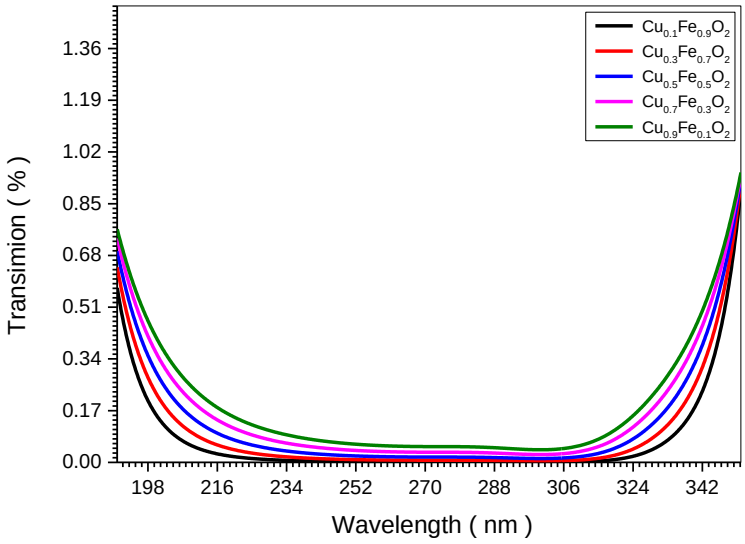

Fig(4.23) relation between transsimion and wavelengths of five ($Cu_x Fe_{(1-x)} O_2$) samples (0.1 ,0.3 ,0.5 ,0.7 and 0.9) Molar concentrations

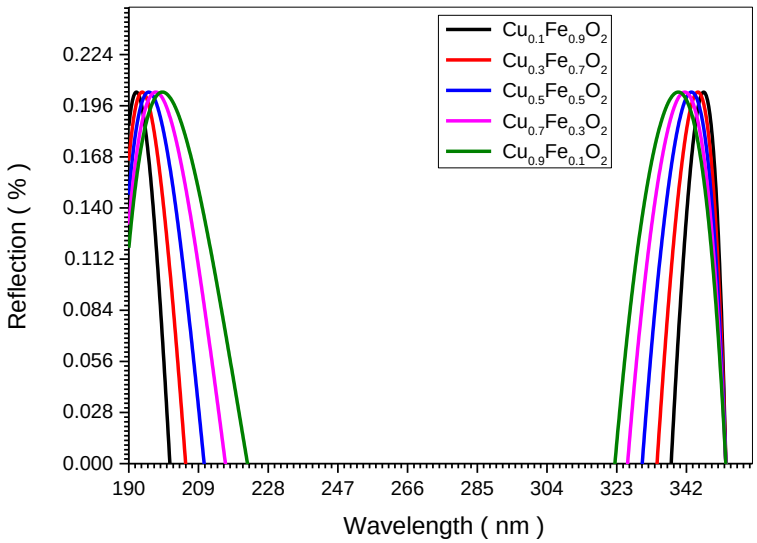

Fig(4.24) relation between reflection and wavelengths of five ($Cu_x Fe_{(1-x)} O_2$) samples (0.1 ,0.3 ,0.5 ,0.7 and 0.9) Molar concentrations

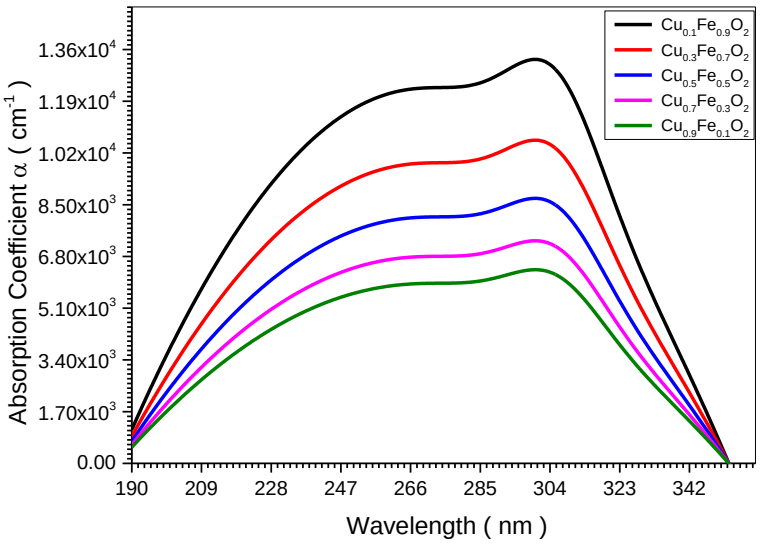

Fig(4.25) relation between absorption coefficient and wavelengths of five ($Cu_x Fe_{(1-x)} O_2$) samples (0.1 ,0.3 ,0.5 ,0.7 and 0.9) Molar concentrations

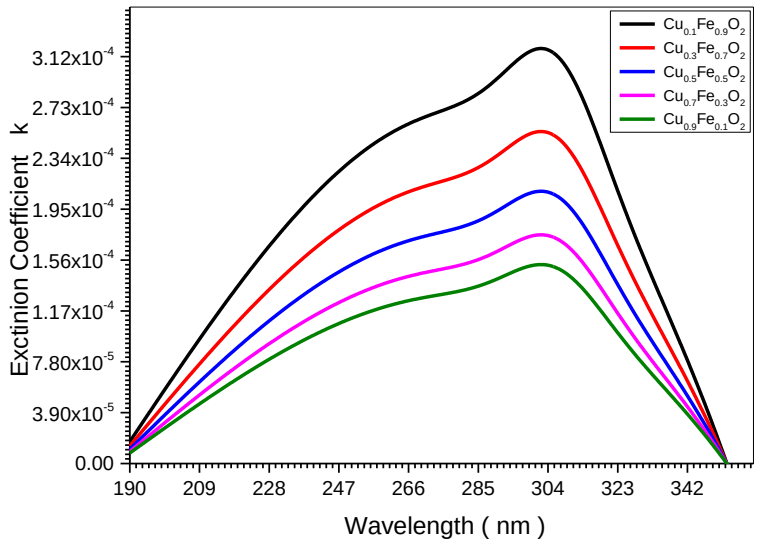

Fig(4.26) relation between exctnion coefficient and wavelengths of five ($Cu_x Fe_{(1-x)} O_2$) samples (0.1 ,0.3 ,0.5 ,0.7 and 0.9) Molar concentrations

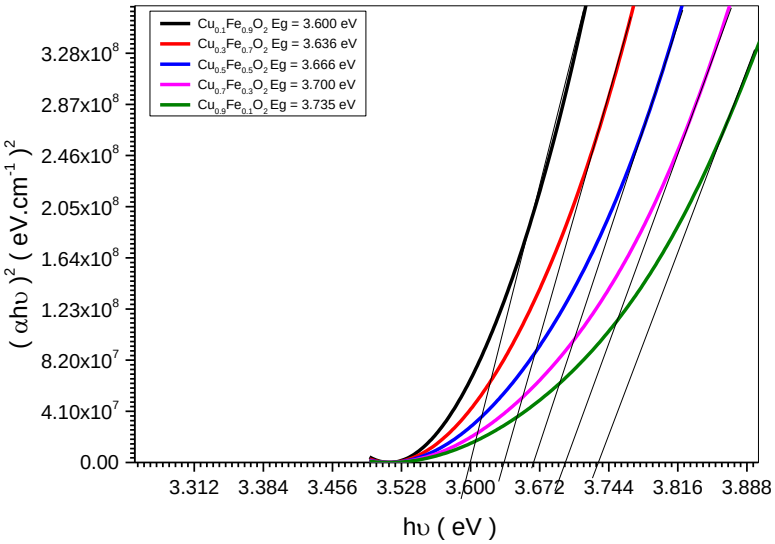

Fig(4.27) optical energy band gap of five ($Cu_x Fe_{(1-x)} O_2$) samples (0.1 ,0.3 ,0.5 ,0.7 and 0.9) Molar concentrations

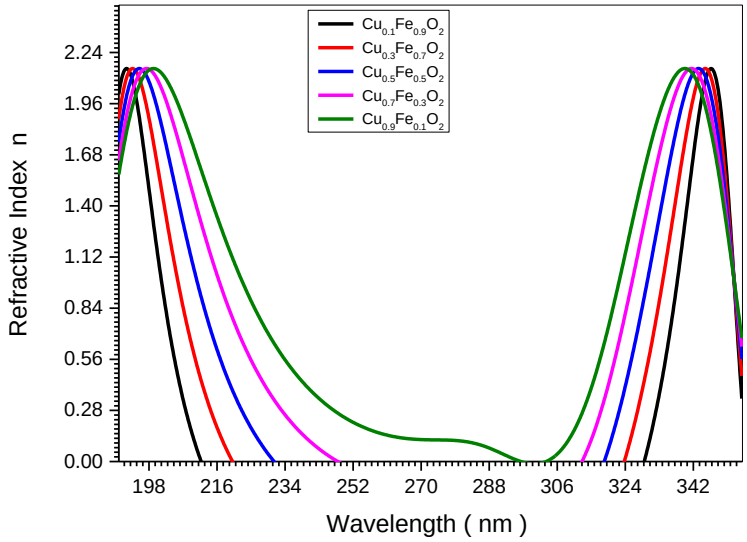

Fig(4.28) relation between refractive index and wavelengths of five ($Cu_x Fe_{(1-x)} O_2$) samples (0.1 ,0.3 ,0.5 ,0.7 and 0.9) Molar concentrations

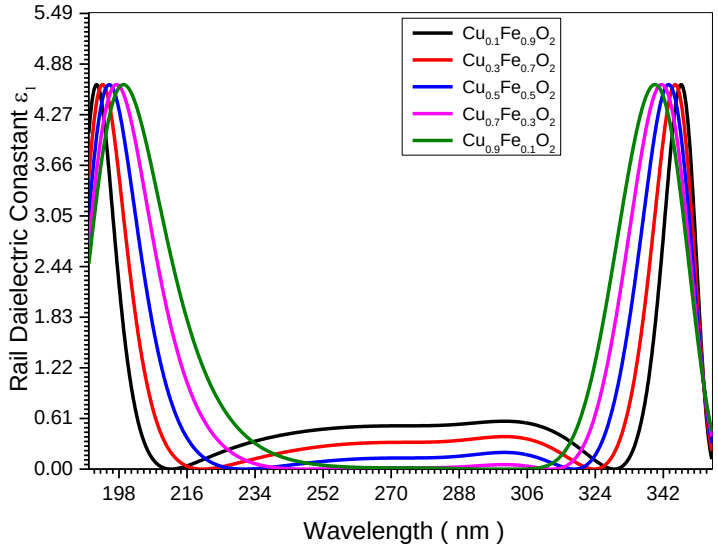

Fig(4.29) relation between rail dialectical constant and wavelengths of five ($Cu_x Fe_{(1-x)} O_2$) samples (0.1 ,0.3 ,0.5 ,0.7 and 0.9) Molar concentrations

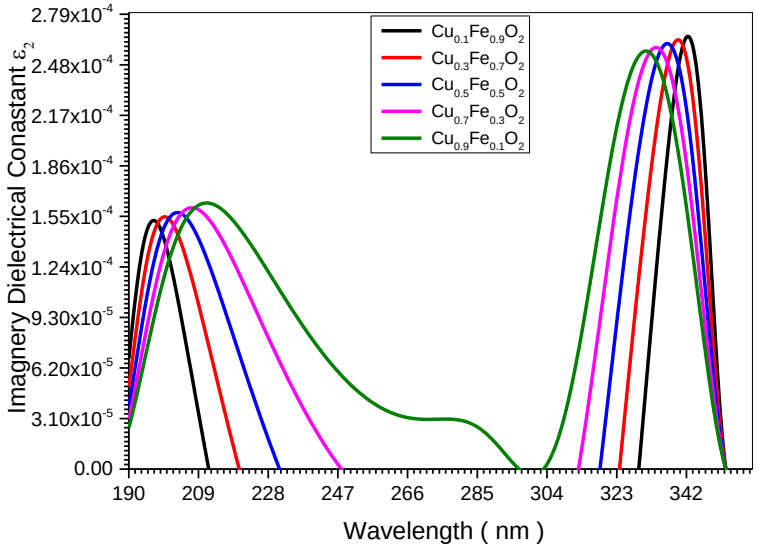

Fig(4.30) relation between imagery dielectcal constant and wavelengths of five ($Cu_x Fe_{(1-x)} O_2$) samples (0.1 ,0.3 ,0.5 ,0.7 and 0.9) Molar concentrations

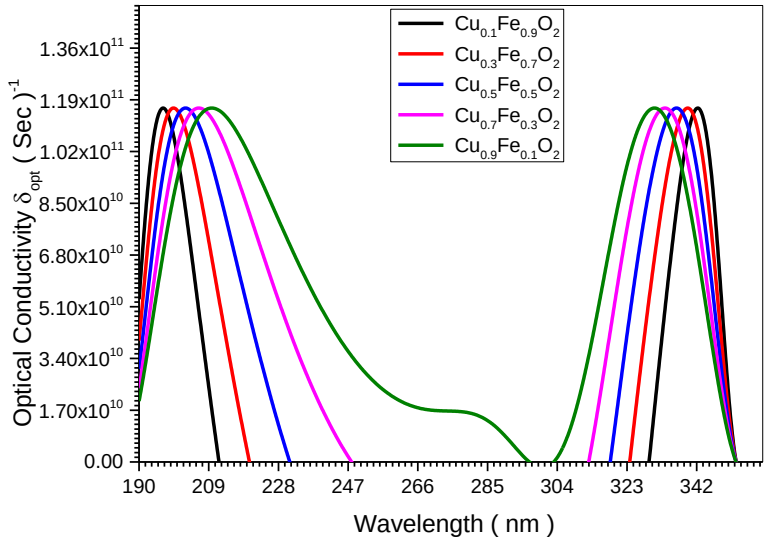

Fig(4.31) relation between optical conductivity and wavelengths of five ($Cu_x Fe_{(1-x)} O_2$) samples (0.1 ,0.3 ,0.5 ,0.7 and 0.9) Molar concentrations

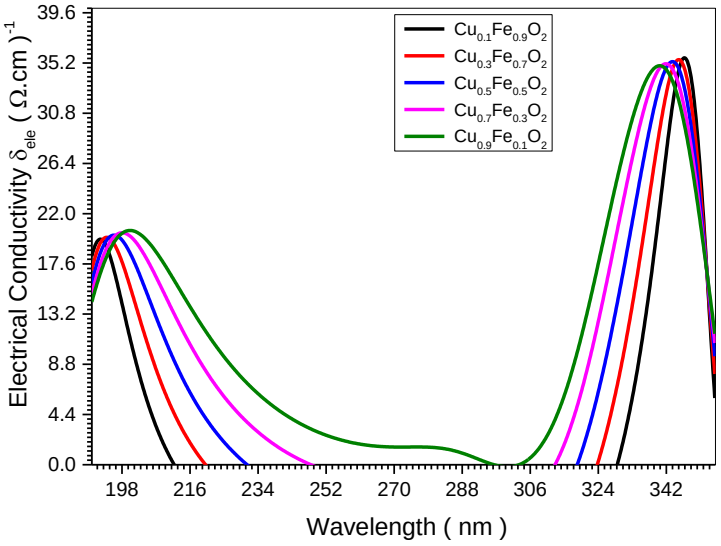

Fig(4.32) relation between electrical conductivity and wavelengths of five ($Cu_x Fe_{(1-x)} O_2$) samples (0.1 ,0.3 ,0.5 ,0.7 and 0.9) Molar concentrations

4.6 Effect of the Nanoscales Size on Electrical and Magnetic Properties Results of ($Al_{2x}Fe_{3(1-x)}O_4$ and $Cu_xFe_{(1-x)}O_2$) samples

The XRD spectra for all samples are displayed in figures.

Table (4.11) optical, electrical and magnetic properties of ($Al_{2x}Fe_{3(1-x)}O_4$) samples

No	Sample	Eg (eV)	n	Opt-Condu(10^{10}(Sec)$^{-1}$	Ele-Condu $(\Omega.cm)^{-1}$	ε 10^{-12} (F/cm^{-1})	μ 10^{-6} (H.cm^{-1})	X_s (nm)
1	$Al_{0.2}fe_{0.9}o_4$	3.667	2.17	9.44	31.14	41.67	0.267	100
2	$Al_{0.6}fe_{0.7}o_4$	3.688	2.13	8.2	30.74	40.15	0.277	78.78
3	$Al_{1.0}fe_{0.5}o_4$	3.712	2.09	6.57	30.07	38.66	0.217	73.88
4	$Al_{1.4}fe_{0.3}o_4$	3.739	2.05	5.78	29.14	37.19	0.299	72.46
5	$Al_{1.8}fe_{0.1}o_4$	3.754	1.95	4.79	28.21	33.65	0.331	69.74

Table (4.12) some optical, electrical and magnetic properties of ($Cu_x Fe_{(1-x)} O_2$) samples

No	Sample	Eg (eV)	n	Opt-Condu(10^{10}(Sec)$^{-1}$	Ele-Condu (Ω.cm)$^{-1}$	ε 10^{-12} (F/cm^{-1})	μ 10^{-6} (H./cm^{-1})	X_s (nm)
1	$Cu_{0.1}Fe_{0.9}O_2$	3.600	1.19	1.3	19.96	12.57	0.88	99.43
2	$Cu_{0.1}Fe_{0.9}O_2$	3.636	1.64	6.2	27.26	23.81	0.47	74.73
3	$Cu_{0.5}Fe_{0.5}O_2$	3.666	1.94	9.4	31.98	33.28	0.33	56.26
4	$Cu_{0.7}Fe_{0.3}O_2$	3.700	2.09	10.9	34.11	38.68	0.29	55.06
5	$Cu_{0.9}Fe_{0.1}O_2$	3.735	2.16	11.6	35.02	41.33	0.27	54.4

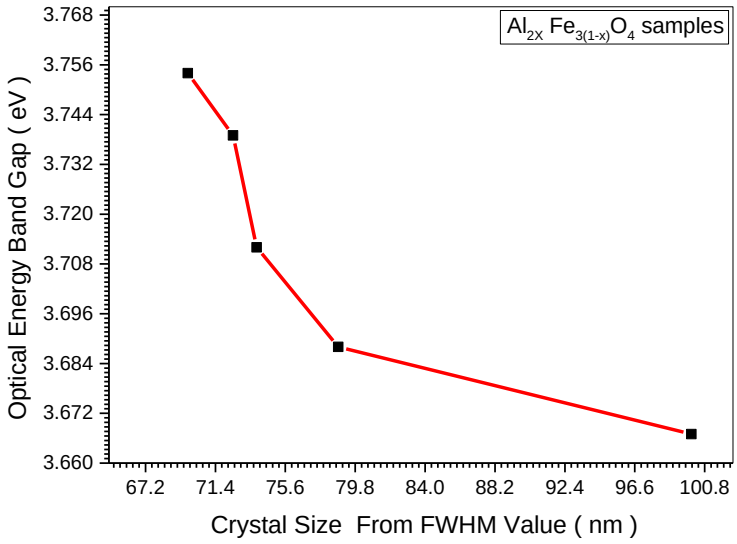

Fig (4.33) relationship between Crystal Size and Optical Energy Band Gap of five ($Al_{2x} Fe_{3(1-x)} O_4$) samples (0.1 ,0.3 ,0.5 ,0.7 and 0.9) Molar

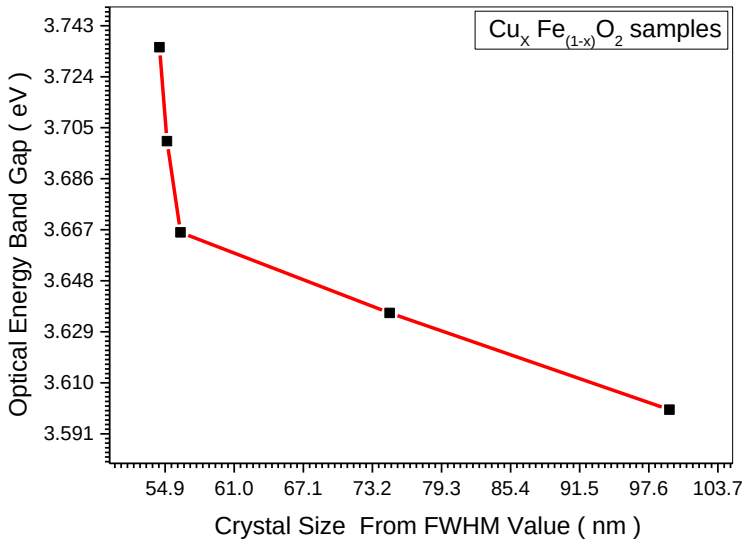

Fig (4.34) relationship between Crystal Size and Optical Energy Band Gap of five ($Cu_x Fe_{(1-x)} O_2$) samples (0.1 ,0.3 ,0.5 ,0.7 and 0.9) Molar

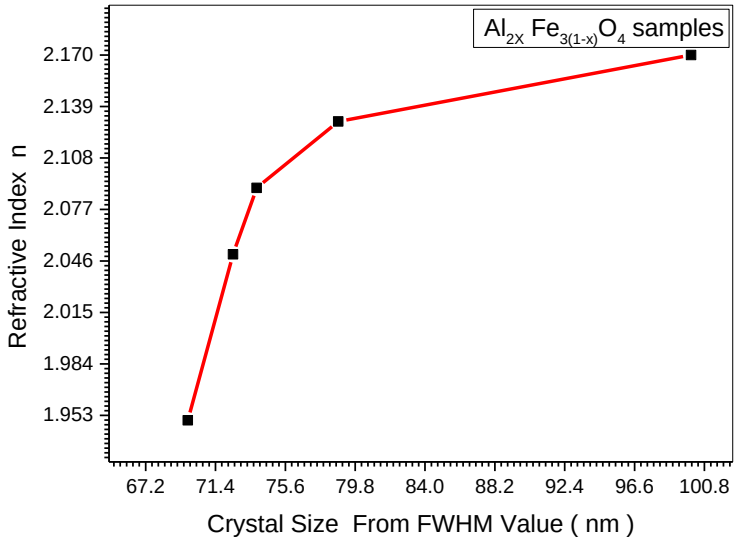

Fig (4.35) relationship between Crystal Size and Refractive Index of five ($Al_{2x} Fe_{3(1-x)} O_4$) samples (0.1, 0.3, 0.5, 0.7 and 0.9) Molar

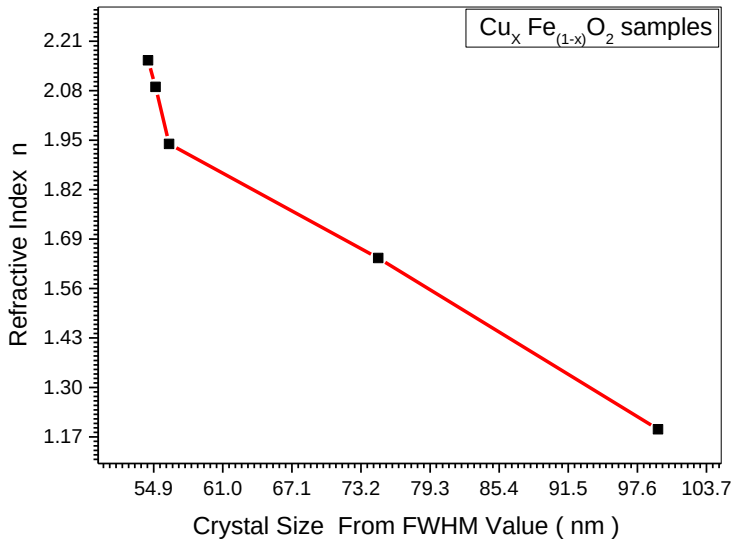

Fig (4.36) relationship between Crystal Size and Refractive Index of five

($Cu_x Fe_{(1-x)} O_2$) samples (0.1 ,0.3 ,0.5 ,0.7 and 0.9) Molar

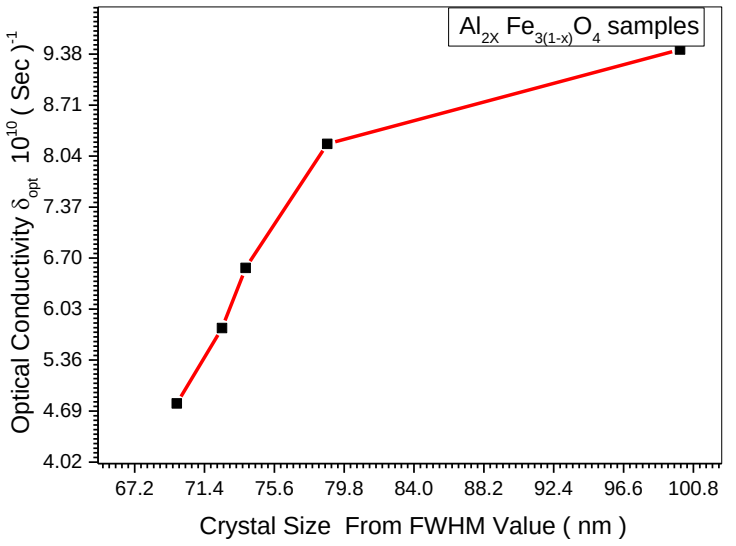

Fig (4.37) relationship between Crystal Size and Optical Conductivity of five

($Al_{2x} Fe_{3(1-x)} O_4$) samples (0.1 ,0.3 ,0.5 ,0.7 and 0.9) Molar

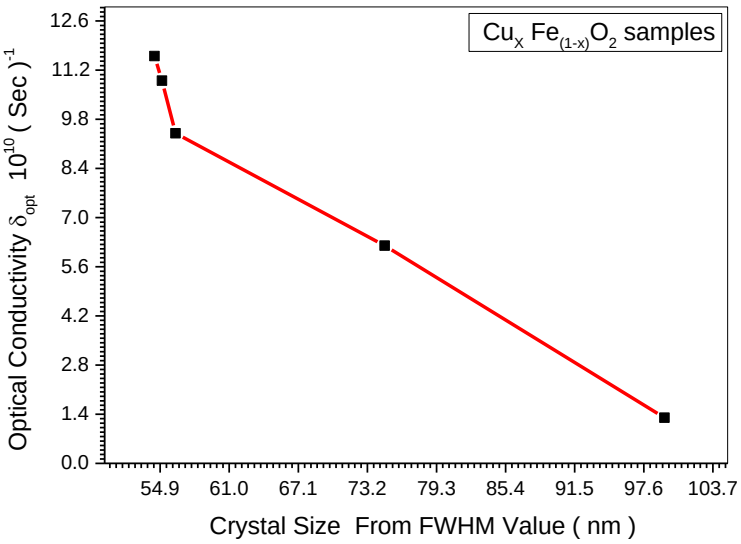

Fig (4.38) relationship between Crystal Size and Optical Conductivity of five

($Cu_x Fe_{(1-x)} O_2$) samples (0.1 ,0.3 ,0.5 ,0.7 and 0.9) Molar

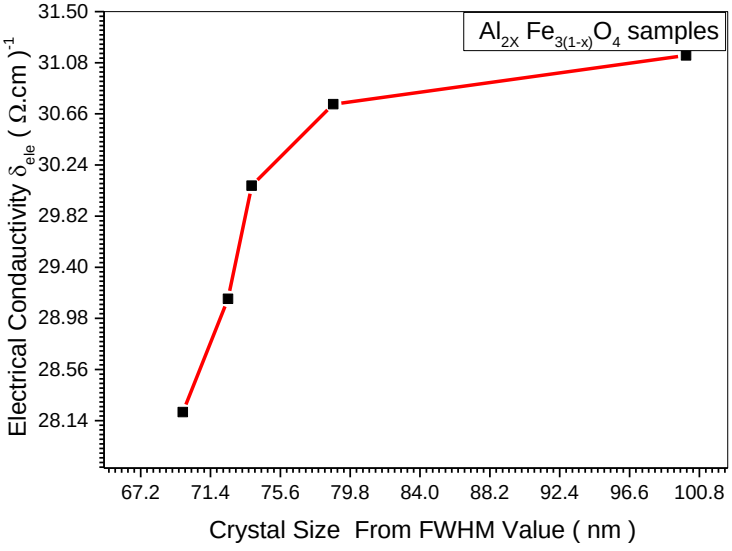

Fig (4.39) relationship between Crystal Size and Electrical Conductivity of five

($Al_{2x} Fe_{3(1-x)} O_4$) samples (0.1 ,0.3 ,0.5 ,0.7 and 0.9) Molar

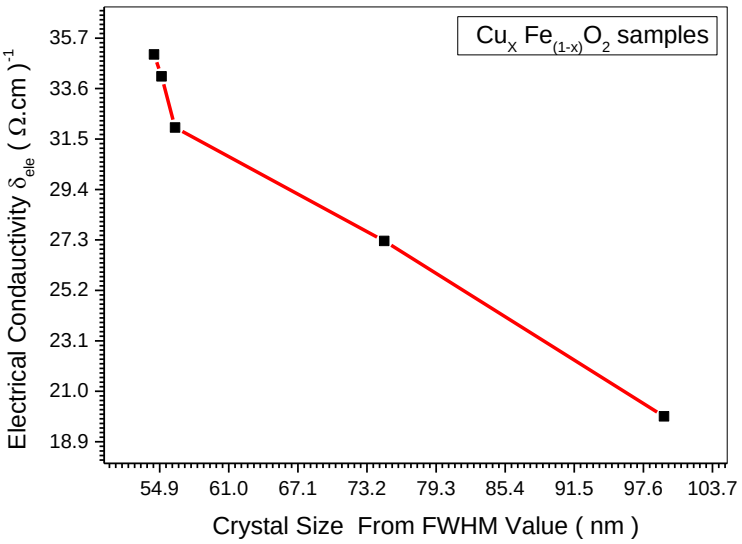

Fig (4.40) relationship between Crystal Size and Electrical Conductivity of five ($Cu_x Fe_{(1-x)} O_2$) samples (0.1 ,0.3 ,0.5 ,0.7 and 0.9) Molar

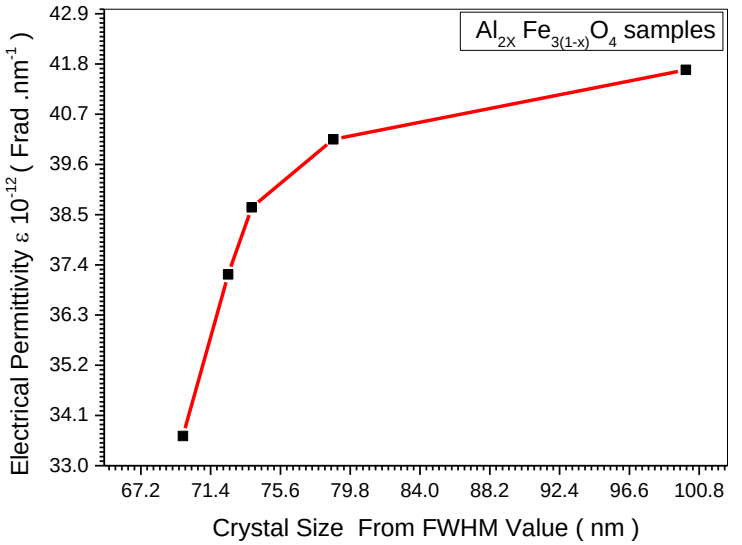

Fig (4.41) relationship between Crystal Size and Electrical Permittivity of five ($Al_{2x} Fe_{3(1-x)} O_4$) samples (0.1 ,0.3 ,0.5 ,0.7 and 0.9) Molar

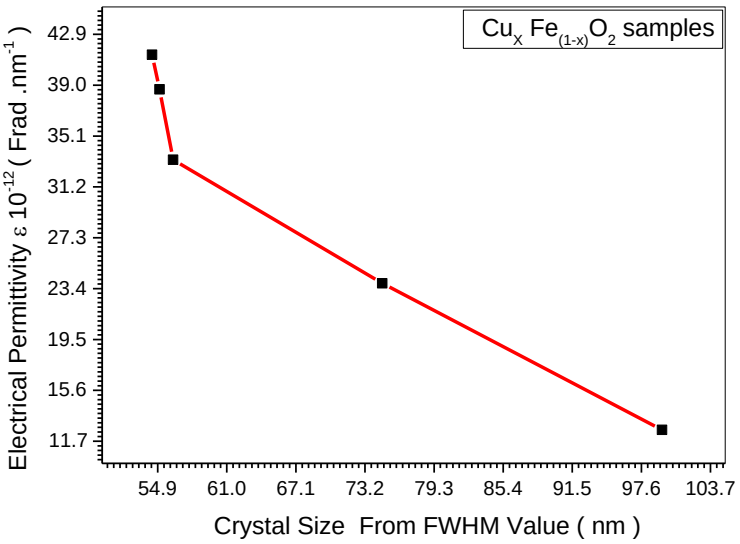

Fig (4.42) relationship between Crystal Size and Electrical Permittivity of five

($Cu_x Fe_{(1-x)} O_2$) samples (0.1, 0.3, 0.5, 0.7 and 0.9) Molar

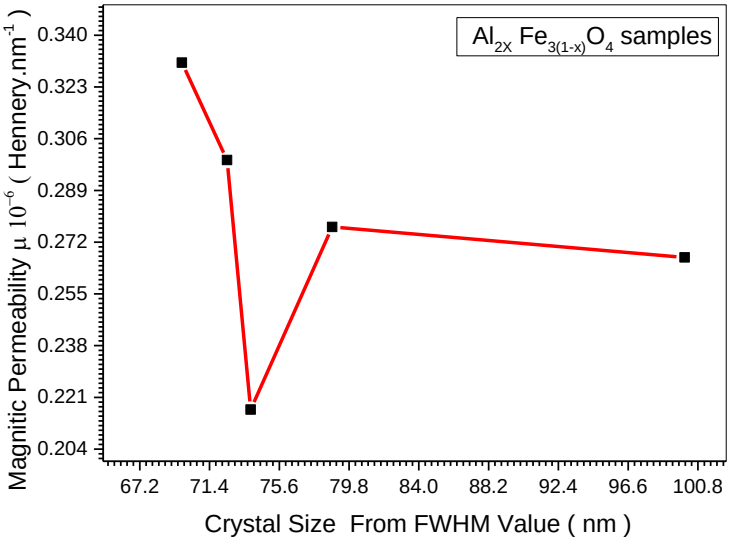

Fig (4.43) relationship between Crystal Size and Magnetic Permeability of five

($Al_{2x} Fe_{3(1-x)} O_4$) samples (0.1 ,0.3 ,0.5 ,0.7 and 0.9) Molar

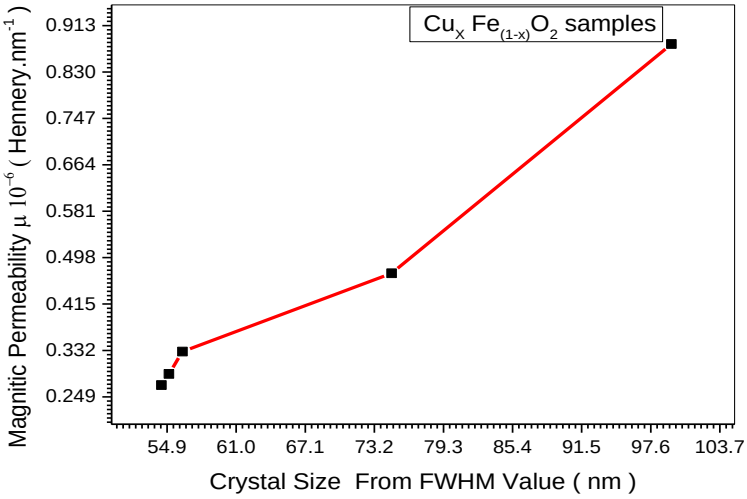

Fig (4.44) relationship between Crystal Size and Magnetic Permeability of five ($Cu_x Fe_{(1-x)} O_2$) samples (0.1, 0.3, 0.5, 0.7 and 0.9) Molar

4.7 FT-IR Analysis

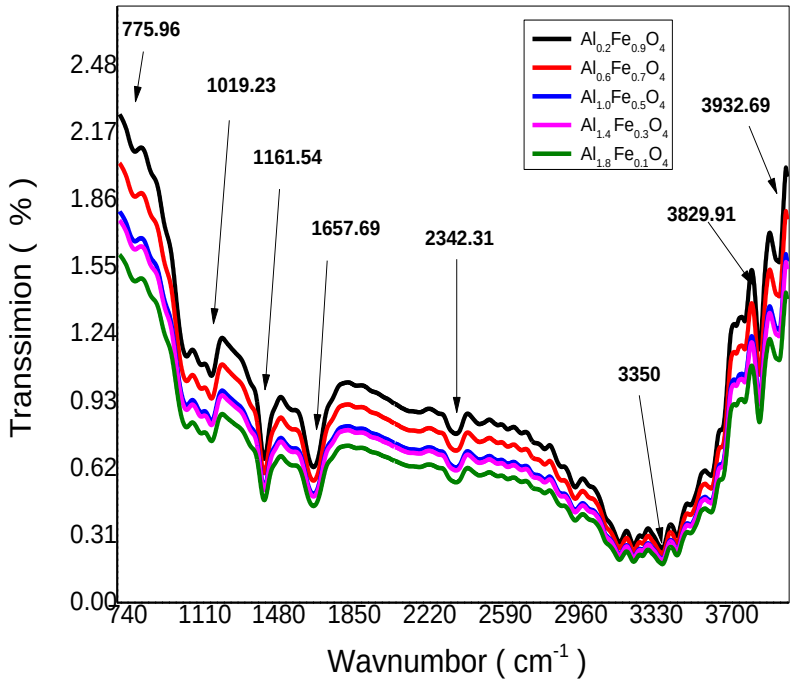

Fig (4.45) ($Al_{2x} Fe_{3(1-x)} O_4$) samples (0.1, 0.3, 0.5, 0.7 and 0.9) Molar concentrations

Table (4.13)

No	Wavenumber (cm^{-1})	Functional Group Names	Type of Vibration
1	775.96	Ortho distributer aromatic	C-H Stretch
2	1019.23	Carbon Bonds	C-X stretch
3	1161.54	Alkoxy	C-O Stretch
4	1657.69	Carboxylic acid	C=O Stretch
5	2342.31	Methane nitrite	CΞN Stretch
6	3350	Alkynes	CΞC Stretch
7	3829.91	Alcohol	O-H Stretch
8	3932.69	Water	O-H Stretch

The infrared spectra of synthesized (Al_{2x} $Fe_{1-x}O_4$) samples were recorded by mattson Fourier Transform Infrared Spectrophotometer in the range of 700 to 4000 cm^{-1} which shown in Fig (4.45). The spectra of all the samples have been used to locate the band positions which are given in the Table (4.13). In the present study the absorption bands ν1, ν2, ν3, ν4, ν5, ν6, ν7 and ν8 are found to be around 775.96 cm^{-1}, 1019.23 cm^{-1} ,1161.54 cm^{-1}, 1657.69 cm^{-1}, 2342.31 cm^{-1}, 3350 cm^{-1}, 3829.91 cm^{-1} and 3932.69 cm^{-1} respectively for all the compositions. The transmittance bands within these specific limits reveal the formation of single-phase spinel structure having two sub-lattices tetrahedral (A) site and octahedral (B) site. The (ν1) band around775.96 cm^{-1} is caused by the Ortho distributer aromatic sides. The band (ν2) around 1019.23 cm^{-1} is due to C-X stretch Carbon Bonds. The band (ν3) around 1161.54 cm^{-1} is associated with the C-O Stretch vibration. The band (ν4) around 1657.69 cm^{-1} is due to C= O stretching. The band (ν5) around 2342.31 cm^{-1} is due to CΞN Stretch stretching. The band (ν6) around 3350 cm^{-1} is associated with the CΞC Stretch vibration. The (ν7, ν8) around 3829.91 cm^{-1} and 3932.69 cm^{-1} is due to the stretching mode of O-H Stretch bending vibration of free or absorbed water and Alcohol which implies that the hydroxyl groups are retained in samples.

4.8 Discussion:

Table (4.11) shows the change of some electrical, magnetic and optical properties of $Al_{2x}Fe_{3(1-x)}O_4$ with x (0.1, 0.3, 0.5,0.7, 0.9). representing the molar

concentration index. According to table (4.11) increasing AL molar concentration decreases the nano crystal size x_s. figure (4.33) indicates that the band gap decreases upon increasing nano crystal size, decreasing AL concentration and increasing Fe concentration. This may be attributed to the fact that increasing Fe concentration which act as magnetic dipole increases the strength of magnetic field which increases in turn the spiting sublevels at the upper and lower edge of the forbidden band leading to increase the number of sub bands inside the forbidden band at the upper and lower edges thus causing narrowing the forbidden band which leads to Eg decrease. According to figure (4.35) the refractive index n increases upon increasing the crystal size and increasing Fe concentration. This may be due to the fact that increasing Fe concentration decreases the speed of light v inside the film as far as Fe is heavier than AL and since $(n = c/v)$. The FTIR analysis for AL shows existence of water, alchol, Methane intrite and carboxylic acid which increases absorption and provides vibrational energies that can be transferred to the carriers.

Figures (4.37) and (4.39) for the optical and electrical conductivity shows an increase of both of them with the nano crystal size. This may be related to the fact that the increase of the crystal size decreases the energy gap thus leading to increase of conductivity. Figure (4.41) shows that the electric permittivity ε increases upon increasing the crystal size. This may be related to the fact the refractive index $(n = c/v = c\sqrt{\mu\varepsilon})$ increases upon increasing the nano crystal size. The change of some electrical, magnetic and optical properties of $Cu_x Fe_{(1-x)}O_2$ for x (0.1, 0.3, 0.5,0.7, 0.9) was exhibited in table (4.12). this table shows that the Nano crystal size decreases upon increasing Cu molar concentration and decreasing Fe molar concentration. According to figure (4.34) the energy band gap Eg decreases upon increasing the Nano crystal size and increasing Fe concentration due to the entrance of sub levels inside the for bidden band as

shown in the discussion of AL. the refractive index in fig (4.36) decreases upon increasing the Nano crystal size, decreasing Cu concentration, and increasing Fe concentration. Since $(n = c/v = c\sqrt{\mu\varepsilon})$ the decrease of Cu concentration decreases the electric permittivity ε as shown in figure (4.42) where the decrease of ε is associated with the increase of the crystal nano size and decrease of Cu concentration. The change of optical and electrical conductivity with the crystal Nano size are shown in figures (4.38) and (4.40) receptivity where the optical and electrical conductivity decreases upon increasing the Nano crystal size and decreasing the Cu concentration. This may be related to the fact that increasing Cu concentration increases considerably the number of free electrons that can enter the conduction band though the energy gap increases. Fig (4.44) indicates that the magnetic permittivity μ increases upon increasing the nano crystal size and Fe concentration this is straight forward as for as increasing Fe concentration which is a magnetic material increases the magnetic permittivity.

4.9 Conclusion:

The increase of AL and Cu molar concentration decreases the Nano crystal size, decreases the energy gap. For AL the increase of Nano crystal size increases the refractive index, optical and electrical conductivity and the electric permittivity. For Cu the reverse takes place where the increase of Nano crystal size decreases the refractive index, optical and electrical conductivity, beside the electric permittivity. He magnetic permeability for Cu increases upon increasing the Nano crystal size.

4.10 Future work:

- This study can be used in improving the performance of solar cells and optical sensors.
- Minerals other than AL and Cu can dope Fe oxides and their electrical, magnetic and optical properties of them can be studied.
- The thermal and mechanical properties of these samples can also be studied.

References:

[1] Serway, Raymond A., and John W. Jewett., Principles of physics. Vol. 1, Saunders (College Pub., USA (1998.

[2] Beiser, Arthur. Concepts of modern physics. Tata McGraw-Hill Education (2003)

[3] Dalven, Richard. "Introduction to applied solid state physics. Topics in the applications of semiconductors, superconductors and the nonlinear optical porperties of solids." New York: Plenum Press (1980).

[4] Seeger, Karlheinz. Semiconductor physics. Springer Science & Business Media, 2013.

[5] Born, Max, and Emil Wolf. "Principles of Optics Second (revised) Edition." Macmillan Co., New York (1964)

[6] G. Burns, Solid State Physics, Academic Press, Inc, London (1985)

[7] David J. Griffith, Introduction to quantum mechanics, prentice Hall, New Jersy (2005). Publishing, califomia (2004).

[8] Levich, B. G., theoretical physics, John wiley and sons, New York (1969).

[9] A. Beiser, concept of modern physics, Mc Graw Hill, London (2002)

[10]Paul Lorrain and Dale R. Corson, Electromagnetic fields and waves, W.H.Ferman and company san Francis co (1970).

[11] Schawbl, F., quantum Mechanics third edition, springer, Berlin (2005).

[12] K. Uuang, Quantum field the Wenham (2010).

[13] Ratna Tantra, Nanomaterial characterization, Wiley & sons, Inc9, New York (2016)

[14]Bhushan, B, Luo, D, Schricker, S.R., Sigmung, W., Zauscher, S., Hand book of Nanomaterials properties, Heidelberg; London, Springer; 2014. ,

[15] Bose, Sarita, Virendra Soni, and K. R. Genwa. "Recent advances and future prospects for dye sensitized solar cells: A review." International Journal of Scientific and Research Publications 5.4 (2015)

[16] Li, B., Wang, L., Kang, B., and Qiu, Y., Solar Energy Materials and Solar Cells, Wiley-VCH, (2006).

[17] Dalveen, Richard. "Introduction to applied solid state physics. Topics in the applications of semiconductors, superconductors and the nonlinear optical porperties of solids." New York: Plenum Press (1980)

[18] .Hassan Karami, synthesis and Characterization of Iron Oxide nanoparticles by solid state Chemical Reaction Method, Tornal of cluster science, March (20210)21:11-20.

[19] G.Aruld has, Quantum Mechanics, and edition, PHI private limited, New Delhi (2009).

[20] Neha Srivastava, Manish Srivastava, P. K. Mishra and Vijai Kumar Gupta. Green Synthesis of Nanomaterials for Bioenergy Applications, First Edition. 2021 John Wiley & Sons Lt8, New York.

[21] Li, B., Wang, L., Kang, B., and Qiu, Y., Solar Energy Materials and Solar Cells, Wiley-VCH, (2006).

[22] Bohren, C., & Huffman, D. (2008). Absorption and scattering of light by small particles (First edit). Arizona: Wiley-Interscience Publishers.]

[23] Shakib, S. A., & Eshrah, I. A. (2011). Electromagnetic Scattering from Conductors: The Recursive Iterative Surface Equivalence Approach. IEEE, (2), 1–4.

[24] Klaus Grobe and Michael Eiselt. (2014). Wavelength division multiplexing; A practical engineering guide. Wiley.

[25] Kamat, P.V., et al., Nanoparticles, in Handbook of Nanostructured Materials and Nanotechnology. Academic Press: New York.2010.

[26] Liu, Xiaolan, et al. "Hybrid energy harvester with bi-functional Nano-wrinkled anti-reflective PDMS film.

[27] Sabu Thomas, Aparna Thankppan, perovskite photovoltaics, 2018 Elsevier Inc.

[28] Shisode, M.V., et al., Investigations of magnetic and ferroelectric properties of multiferroic Sr-doped bismuth ferrite. Applied Physics A, 2018. 124(9): p. 603

[29] Gibin George, Zhiping Luo, Sivosanara Roo Ede fundamentals of perovskite Oxides, 2020 by CRC Press.

[30] Bhandari, K.P., R.J. An overview of Hybrid –organic – inorganic metal Halide perovskite solar cells. Academic Press: Cambridge, MA, USA, 2018, pp.233-254.

[31] Richard J. D. Tiley, perovskite: structure – property relationships, first published 2016 Wiley & sons, Inc. ISBN 97811189535651

[32] Bhoyar, D.N., et al., Structural, infrared, magnetic and ferroelectric properties of Sr0· 5Ba0· 5Ti1-xFexO3 Nano ceramics: Modifications via trivalent Fe ion doping. Physical B: Condensed Matter, 2020. 581: p. 411944.

[33] Amira Jad Elrb Ali, Mubarak Dirar Abdallah, Abdalsakhi S M.H, A. E. Mohamed Osman, Ahmed H .Alfaki, Asim Ahmed Mohamed Fadol, Asma, Abd-Alla Mohamed Altambor, Syntheses (Ba x Fe1-x Ti O 4) Nano size and Study Crystal properties, Optical Energy Gap and Optical & Electrical Conductivity, IOSR Journal Of Applied Physics (IOSR-JAP)

[34] Brinker,c.Jeffrey , sol –gel science :the physics and chemistry of sol-gel processing “, Boston, academic press, 2019.

[35] M. K. Jararaj, Nano structured Oxide and Devices: Optical and Electrical Properites1st ed. 2020 springer.

[36] Ye, Z.-G., Handbook of advanced dielectric, piezoelectric and ferroelectric materials: Synthesis, properties and applications. Elsevier, 2008

[37] Amira Jad Elrb Ali, Mubarak Dirar Abdallah, Abdalsakhi S M.H, A. E. Mohamed Osman Ahmed H .Alfaki, Asim Ahmed Mohamed Fadol, Asma Abd-Alla, Mohamed Altambor, The Effect of Fe Concentration on Crystal size, Crystal Spacing, Nano Size, and Absorption Coefficient for (Ba x Fe1-x Ti O4), IOSR Journal of Applied Physics (IOSR-JAP) e-ISSN: 2278-4861.Volume 13, Issue 6 Ser. II (Nov. – Dec. 2021), PP 14-18

[38] Chen, K., Chen, X., Xue, D., Hydrothermal route to crystallization of FeOOH nanorods via FeCl36H2O: effect of Fe3+ concentration on pseudo capacitance of iron-based materials, 2015.

[39] Arico AS, Bruce P, Scrosati B, Tarascon J-M, Schalkwijk WV Nanostructured materials for advanced energy conversion and storage devices. (2005) Nat Mater 4:366–377.

[40] Claassen, J.O., Sandenbergh, R.F. Influence of mixing on the quality of iron precipitates in zinc-rich solutions. Hydrometallurgy. (2007)

[41] Zohal E. M. Ebnouf, Mahmoud. Hilo, Mubarak Dirar Abdallah, Ahmed Alfaki, Abdalsakhi S M.H & Sawsan Ahmed Elhouri Ahmed, The Effect of Changing Concentrations of Al2O3 On The (ZnO)X(Al2O3)1-X Thin Films Absorption and Energy Gap, International Journal of Scientific Engineering and Applied Science (IJSEAS) – Volume-3, Issue-3, March 2019.

[42] Guang Zhu, Likun Pan, perovskite materials: synthesis, characterization, properties and application BoD- books on Demand, 2016.

[43] brinker, c. Jeffrey, sol –gel science: the physics and chemistry of sol-gel processing ", Boston, academic press ,2019

[44] M. K. Jararaj, Nano structured Oxide and Devices: Optical and Electrical Properites1st ed. 2020 springer.

[45] M. Dehghanab and A. Behjat *ab, Deposition of zinc oxide as an electron transport layer in planar perovskite solar cells by spray and SILAR ethods comparable with spin coating, RSC Adv., 2019, 9, 20917–20924.

[46] A. K. Chandiran, A. Yella, M. T. Mayer, P. Gao, M. K. Nazeeruddin and M. Gratzel, Adv. Mater., 2014, 26, 4309–4312.

[47] T. Sahoo, M. Kim, M.-H. Lee, L.-W. Jang, J.-W. Jeon, J. S. Kwak, I.-Y. Ko and I.-H. Lee, J. Alloys Compd., 2010, 491, 308–313.

[48] H.-S. Kim, C.-R. Lee, J.-H. Im, K.-B. Lee, T. Moehl, A. Marchioro, S.-J. Moon, R. Humphry-Baker, J.-H. Yum, J. E. Moser, M. Gr¨atzel and N.-G. Park, Sci. Rep., 2012, 2, 591.

[49] Sakina Ibrahim Ali, Mubarak Dirar Abdallah, Sawsan Ahmed Elhouri Ahmed, The Relationship Between Energy Gab & Efficiency in Dye Solar Cells, International Journal of Current Trends in Engineering & Research (IJCTER) e-ISSN 2455–1392 Volume 2 Issue 7, July 2016 pp. 82 – 89.

[50] Hino, Y., Kajii, H. & Ohmori, Y. 2006. Transient characteristics of polyfluorene-based polymer light-emitting diodes and their application for color tunable devices.

[51] Hoke, E. T. Vandewal, K., Bartelt, J. A., Mateker, W. R., Douglas, J. D., Noriega, R., Graham, K. R., Fréchet, J. M., Salleo, A. & McGehee, M. D. Recombination in Polymer:Fullerene Solar Cells with Open-Circuit Voltages Approaching and Exceeding 1.0 V. Adv. Energy Mater. 3,220–230 (2013).

[52] Hino, Y., Kajii, H. & Ohmori, Y. 2006. Transient characteristics of polyfluorene-based polymer light-emitting diodes and their application for color tunable devices. Thin Solid Films.

[53] Azza Abdalwahab Abdalla, Ali Sulaiman Mohamed, Mubarak Dirar Abdallah, Abdalsakhi Suleman & Sawsan Ahmed Elhouri Ahmed, The Effect of

[54] Physical properties of carbon nanotubes by Saito, Dressel Haus and Dressel Haus (Imperial College Press, 1998).

[55] Carbon Nanotubes, basic concepts and physical properties by Reich, Thomsen and Maultzsch (Wiley, 2004).

[56] Introduction to Carbon Nanotubes and Its Applications in Semiconductor Industry Author: Lo, SiO-On 5/10/2006.

[57] L. Solymar, D. Walshr R. R. A. Syms, electrical properties of materials, Ninth edition Oxford University Press, 2014, ISBN 978–0–19–870278–8.

[58] M. K. Jayaraj, optical and electrical properties, material Horizons; from nature to nanomaterial, 1st edition 2020, ISBN. 10-98115333x.

[59] Michael B. Heaney. "Electrical Conductivity and Resistivity."Copyright CRC Press LLC. 2000.

[60] Baumeister PW, Optical absorption of cuprous oxide, Physical Review,1961.

[61] E.Y.Tsymbal, Optical properties of solids, academic press New York and London, 1972.

[62] Gonzale, W and Mancini, H.L, an introduction to materials science. Princeton university press (2004). ISBN 9780-691-07097-1

[63] Gunzler, H. and Gremlich, H.-U., IR Spectroscopy: An Introduction, Wiley-VCH, Weinheim, Ger-many, 2002.

[64] Hollas, J. M., Modern Spectroscopy, Wiley, Chichester, UK, 3rd Edition, 1996.

[65] N.B. Colthrup, L.H. Daly, S.E. Wiberley, Introduction to Infrared and Raman Spectroscopy, Academic Press, Sandie goes, 1990.

[66] J. O. Carneiro. S. Azevedo, F. Fernandes, E. Freitas, M. Pereira, C. J. Tavares, and S. Lanceros-Mendez and V. Synthesis of iron-doped TiO2nanoparticles by ball-milling process: the influence of process parameters

on the structural, optical, magnetic, and photocatalytic properties, Springer Science+ Business Media New York 2014.

[67] Duangdao Channei1, Auppatham Nakaruk, Sukon Phanichphant, Pramod Koshy and Charles Christopher Sorrell. Effect of iron doping on the structural and optical properties of CeO2films, Springer Science and Business Media New York 2016.

[68] Stephen Lourduraj and Rayar Victor Williams Effect of iron doping on structural and optical properties of TiO2 thin film by sol–gel routed spin coating technique J. Adv. Dielect. 7, 1750024 (2017).

[69] BS Avinash, VS Chaturmukh, HS Jayanna, and CS Naveen, effect of particle size on band gap and DC electrical conductivity of TiO_2 nanomaterial,2016.

[70] L.H Omari and H. Lassri, Structural and optical properties of Fe-doped ruddlesden – popper Ca3 Ti_{2-x} Fe_x $O_{7-\delta}$ nanoparticles Elsevier B. V. 2020.

[71] Nicholas O. On Gwen, Andrew O. Oduor1, and Elijah O. Ayieta, Effect of Concentration of Reactants on the Optical Properties of Iron Doped Cadmium Stannate Thin Films Deposited by Spray Pyrolysis; Published by Scientific & Academic Publishing 2019.